Chaos and transport properties of adatoms on solid surfaces

2002 J. Phys.: Condens. Matter 14 6191

(http://iopscience.iop.org/0953-8984/14/24/316)

INSTITUTE OF PHYSICS PUBLISHING JOURNAL OF PHYSICS: CONDENSED MATTER

J. Phys.: Condens. Matter **14** (2002) 6193–6232 PII: S0953-8984(02)34891-4

Chaos and transport properties of adatoms on solid surfaces

J L Vega, R Guantes and S Miret-Artés

Instituto de Matemáticas y Física Fundamental, CSIC, Serrano 123, 28006 Madrid, Spain

E-mail: jlvega@imaff.cfmac.csic.es, rgn@imaff.cfmac.csic.es and salvador@fam10.imaff.csic.es

Received 14 March 2002
Published 31 May 2002
Online at stacks.iop.org/JPhysCM/14/6193

Abstract

Some aspects of the theory of transport in chaotic Hamiltonian systems are reviewed and applied to a model potential for diffusion of Na atoms on a Cu(001) surface (Graham A P, Hofmann F, Toennies J P, Chen L Y and Ying S C 1997 *Phys. Rev. Lett.* **78** 3900). Through a detailed investigation of the deterministic dynamics, we describe how normal and anomalous diffusion can take place, as well as the influence of the chaotic dynamics on the short-time dynamical behaviour of the system and on the existence of long jumps. The theoretical aspects of atom–surface diffusion relevant to experiments are also reviewed and connected to some statistical models used to describe diffusion in chaotic Hamiltonian systems.

Contents

0953-8984/02/246193+40$30.00

1. Introduction

The diffusion of atomic and molecular adsorbates is one of the most elementary processes taking place on surfaces. Its study is important both for practical and conceptual reasons. On one hand, the diffusion of the adsorbates is a preliminary step in more complex surface phenomena such as associative desorption and heterogeneous catalysis, and strongly affects their overall efficiency. The need for quantitative and accurate knowledge of diffusion coefficients or rates, as well as a detailed characterization of diffusion mechanisms and adsorbate–substrate interactions, has stimulated considerable progress in experimental techniques. There are different techniques available nowadays for obtaining accurate diffusion coefficients and frequencies of adsorbates vibrations, each one with different ranges of applicability and advantages. There is also a large body of literature on these techniques and the information that it is possible to obtain from them; see for instance the reviews [1–4]. On the other hand, the basic theory behind atomic and molecular diffusion is conceptually very rich, with important implications for different branches of physics, chemistry, and mathematics. In general there are a number of different possible views of the same process and, depending on the specific case, they can be equally valid, or one more appropriate than others. For instance, a diffusion process can be considered as a problem of Brownian motion, whose theory dates back to works by Einstein, Smoluchowski, Langevin, Rayleigh, Fokker, Planck, and others at the beginning of the last century. That is, the diffusing particles follow stochastic paths influenced by a random force coming from the huge number of degrees of freedom of a large heat reservoir. The theory of stochastic processes was generalized and put on firm mathematical grounds some time later by Stratonovich and Îto, and its foundations in probability theory were also established by a number of mathematicians. This approach can be supplemented by the existence of an external force field, as is the case for atomic diffusion on a surface when considering the adiabatic particle–surface interaction potential. But atomic or molecular diffusion can also be seen as a problem of activated escape over a potential barrier. This line of thinking was initiated in the famous work of Kramers in 1940 [5] and it is still active, having led to a large number of theoretical works and developments; see for instance the reviews [6, 7]. While the first approach is intimately linked to non-equilibrium statistical mechanics and hydrodynamics, the second one is very much related to the transition state theory of chemical reactions. Here we will consider diffusion intrinsically as a dynamical problem, and when long-time adsorbate motions are involved, non-commutation rules can be ignored. In this sense, classical mechanics together with statistical physics applies naturally.

There is yet another view which comes from a simplification of the stochastic approach, by assuming the coupling to the environment or the thermal bath in equilibrium to be negligible, and considering as a starting point only the dynamics ruled by Newton's equation. Although conceptually it was Boltzmann's original idea to deduce thermodynamics from the classical microscopic equations of motion, for small systems with only a few degrees of freedom this has been finding rigorous justification only in the last few decades, with the development of the ergodic theory of non-linear dynamical systems [8].

It is not our intention to devote this review to the theory of chaotic transport, on which good recent books and reviews exist [9–11], nor to particular experimental and theoretical approaches to atom–surface diffusion that have been described at length elsewhere. We find that most of the combined experimental and theoretical works on atom–surface diffusion have

been based on the first two, more traditional, points of view, while theoretical developments of non-linear transport theory have been mainly applied to simple models amenable to analytical treatment, but difficult to subject to experimental verification. Our aim is to partially bridge the gap between the two worlds by choosing a prototype system, well studied experimentally and theoretically within the stochastic approach, and investigate in detail what kind of transport can be induced by the deterministic dynamics, to characterize the mechanism for such transport and consider its possible connection to real experiments. In doing so, we show that anomalous non-Brownian transport can usually arise due to the underlying chaotic dynamics. We will study the mechanism for anomalous transport in detail and relate it to some statistical models proposed. We will also derive some original results in connecting these models to quantities of interest in real experiments, in particular to the quasielastic helium-atom scattering (QHAS) technique.

The organization of the review is as follows. After briefly describing in the next section the model system employed, which has been previously established and used in theoretical and experimental QHAS studies [12], we perform a complete investigation of the chaotic dynamics of this system in section 3. First, we introduce the relevant theory in what we hope will be an accessible way and then apply it to our model, emphasizing the essential physical picture emerging from this study. We will also relate in this section the chaotic dynamics to the vibrational (non-diffusive) motion of the adparticles, which can be studied experimentally by the same technique. The investigation of the transport of the adparticles will start in section 4. After some generalities about Brownian motion, we will describe the basic theory behind the QHAS technique and its connection to the stochastic point of view. The deterministic diffusion of our system in the Brownian diffusion regime will also be studied and related to the chaotic dynamics. Section 5 is devoted to the anomalous transport regime, which can be induced by the deterministic dynamics under some circumstances. Anomalous transport is by now recognized not as a pathological phenomenon, but as a fairly general process supported by experimental evidence in different physical systems. Nevertheless, as it is still much less known than Brownian transport, we will describe its origins in detail. From the different possible approaches, we choose one that is appropriate for making the connection to the deterministic dynamics and to relevant quantities of the QHAS experiments. We also discuss in this section the influence of dissipation and noise through the coupling to the thermal bath. Section 6 points out some important conclusions and problems to be addressed in the future concerning this topic.

2. Model system and potential

The diffusion of Na atoms at different coverages on a Cu(001) surface has been recent and extensively investigated experimentally with the QHAS technique, as well as theoretically within the Langevin and Fokker–Planck (FP) formalisms [12–14]. At low coverages of Na atoms, the adsorbate–adsorbate interactions can be disregarded and the corresponding experimental features have been interpreted only in terms of the adsorbate–substrate interaction governed by a non-separable potential energy surface (PES), whose parameters were fitted to experimental results using molecular dynamics simulations in reference [12]. This PES describes the systematic or adiabatic force affecting the Na atoms, which can be added to the random force due to the thermal vibrations of the surface.

Since the vibrations of the Na adatoms normal to the surface have a much higher frequency [15] than those parallel to the surface (the *frustrated translational mode* or T mode), the adiabatic interaction potential is considered as being averaged over the normal vibrations. Therefore the substrate potential is a two-dimensional function of only the in-plane coordinates x and y:

$$V(x, y) = V_0(x, y) + V_1(x, y) + V_2(x, y). \tag{2.1}$$

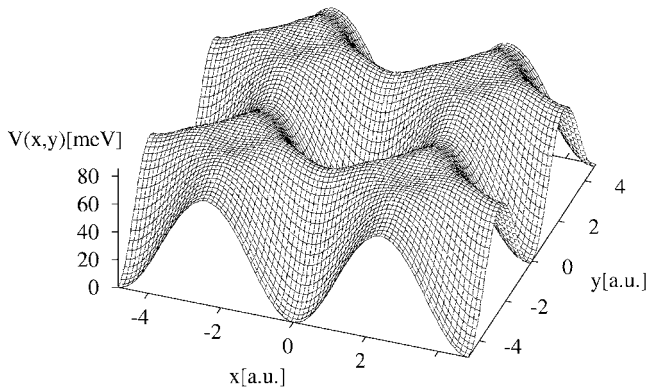

Figure 1. The Na/Cu(001) interaction potential. The zero of the energy axis is taken at the energy of the hollow-site minima ($x = y = 0, \pm a, \ldots$). The x- and y-directions correspond to the [1$\bar{1}$0] and [110] azimuths, respectively, and the barrier for motion along this direction is 74.64 meV. The diagonal directions have Miller indices [100] and [010] and the energy barrier is at 84.49 meV.

The first term is a simple separable cosine potential:

$$V_0(x, y) = V_0[2 - \cos(2\pi x/a) - \cos(2\pi y/a)] \tag{2.2}$$

where a is the lattice constant of the Cu(001) surface ($a = 2.557$ Å), and $V_0 = 41.4$ meV. The second term is added to produce a lowering of the potential barrier at on-top sites according to the observations

$$V_1(x, y) = -A \sum_{m,n} \exp(-b\{[x/a - (m + \tfrac{1}{2})]^2 + [y/a - (n + \tfrac{1}{2})]^2\}) \tag{2.3}$$

with $A = 2V_0$ and $b = 11.8$. Finally, the third term is a non-separable part which changes the curvature near the minima and varies the difference between the potential at the minima and the bridge positions:

$$V_2(x, y) = CV_0\pi^2 \sum_{m,n} [(x/a - m)^2 + (y/a - n)^2] \exp[-(x/a - m)^2 - (y/a - n)^2] \tag{2.4}$$

with $C = -0.2$. Note that for a periodic potential, the sums in (2.3) and (2.4) must run over the entire set of integer pairs (m, n). In practice, for the classical trajectory simulations, we reduce the dynamics to a single Wigner–Seitz cell by imposing periodic boundary conditions, and the sum over Gaussians is truncated at some few terms (typically m and n vary between -10 and 10). In figure 1 we show a 3D plot of the corresponding PES. The x- and y-directions are taken along the azimuths with Miller indices [1$\bar{1}$0] and [110], respectively. The energy zero is taken at the minima of the potential wells corresponding to hollow sites. The saddle-point barrier along the x- or y-directions is at 74.64 meV, and the saddle-point barrier along the diagonal [100] or [010] azimuths is at 84.49 meV. The small minima on the potential truncated hills correspond to on-top sites above the copper atoms and are at energy 82.74 meV. As will be shown later, they will also play a role in the classical dynamics and can be responsible for the anomalously high rate of migration paths along the diagonal [100] direction detected in the experiment [12]. The maxima at the top hills are located at 85.51 meV.

An important feature of the present PES is its non-separability, as opposed to a previous PES used to reproduce the experiments [13, 16]. The separable PES could not explain all the experimental findings—in particular, the marked anisotropy in diffusion along different directions. The non-separability of the adiabatic potential can influence considerably the occurrence of long jumps and the dependence of the diffusion coefficient on friction [16, b].

3. Chaotic dynamics

Chaotic dynamics, or sensitivity to initial conditions, appears generically in dynamical systems obeying non-linear differential equations. For autonomous (time-independent) Hamiltonian systems, chaotic dynamics is possible with at least two degrees of freedom. Whenever we can write the Hamiltonian as the sum of a kinetic energy part, depending only on the momenta, and a potential energy part, a necessary condition for the existence of chaotic dynamics is the non-separability of the potential energy function. Since the systematic atom–surface interaction is usually described by a two- or three-dimensional non-separable PES [12, 17, 18], the deterministic atom–surface dynamics is generally expected to be chaotic.

Usually the phase space of a chaotic Hamiltonian system consists of regions of partial integrability, characterized by the existence of tori and dynamical stability, with interspersed regions of chaotic behaviour. This behaviour has its origin in the dynamical instability caused by the homoclinic and heteroclinic intersections of manifolds of unstable periodic motions [19–21]. By changing a parameter of the Hamiltonian, like some coefficient in the potential energy function or the total energy in the case of a conservative system, the degree of chaos (or irregularity) of a system can be varied. It can range between complete integrability, where no dynamical instability is present, and hyperbolicity (where all the periodic motions are unstable) which implies ergodicity. The consequences of this intrinsic random behaviour (intrinsic because it is generated by the deterministic equations of motion, without the need to introduce any external 'environment' or fluctuations) are far reaching. For instance, a complete description of the motion is generally impractical, and we can look for a statistical approach. That is, the evolution and relaxation towards equilibrium of certain average quantities can be studied, rather than the trajectory corresponding to a given set of initial conditions. Chaos provides here a natural justification for the introduction of statistical ensembles. Since chaos may already appear in Hamiltonian systems with only two degrees of freedom, statistical mechanics can be justified for small classical systems. The presence of many particles is not a basic requirement for the foundation of statistical mechanics, and in particular for the existence of transport. As a consequence, great interest, also promoted by the advances in the mathematical tools needed in ergodic theory of dynamical systems, is being aroused by the study of transport properties of chaotic systems [9].

Apart from its fundamental importance in disciplines such as non-equilibrium statistical mechanics, where chaos can provide a connection between the irreversible phenomenological macroscopic equations and the reversible Hamiltonian equations [10], deterministic chaos can also induce transport mechanisms not considered in conventional statistical mechanics. For instance, the possibility of anomalous transport (mean squared displacements (MSDs) growing faster or slower than linearly in time) will be considered below.

3.1. Dynamical properties of chaotic Hamiltonian systems

The dynamics is governed by the set of first-order differential equations

$$\dot{\boldsymbol{x}} = \boldsymbol{F}(\boldsymbol{x}), \tag{3.1}$$

where $\boldsymbol{x}$ is a point of the phase space of the system. Equivalently, the individual trajectories in phase space are given by the mapping

$$\boldsymbol{x} = \boldsymbol{\Phi}^t(\boldsymbol{x}_0) \tag{3.2}$$

where $\boldsymbol{\Phi}^t$ is the evolution rule, called the *flow*, that tells us where the initial points in phase space $\boldsymbol{x}_0$ have moved to after a time t. In general it is a non-linear function of the initial conditions and time.

As remarked above, we can seek for a statistical description of the dynamics and study the evolution of statistical ensembles of trajectories. Then we can define a probability density in phase space given by

$$f(\boldsymbol{x},t)=\lim_{N\to\infty}\frac{1}{N}\sum_{i=1}^{N}\delta(\boldsymbol{x}-\boldsymbol{x}_i(t)) \tag{3.3}$$

where the trajectories $\boldsymbol{x}_i(t)$ are solutions of equations (3.1) or (3.2) with different initial conditions. Applying the principle of conservation of probability, this density can be shown to obey a continuity equation:

$$\partial_t f(\boldsymbol{x},t)=-\boldsymbol{\nabla}\cdot(\boldsymbol{F}(\boldsymbol{x})f(\boldsymbol{x},t)) \tag{3.4}$$

determining the time evolution of the probability density, known as the Liouville equation.

The evolution of the phase-space volume is controlled by the Jacobian determinant of the transformation (3.2) which is easily expressed, formally solving (3.1) and using (3.2), as

$$|\det\partial_{\boldsymbol{x}}\boldsymbol{\Phi}^t|=\exp\int_0^t\boldsymbol{\nabla}\cdot\boldsymbol{F}\,\mathrm{d}\tau. \tag{3.5}$$

For Hamiltonian systems the phase-space volume is preserved and the divergence of the vector field vanishes, $\boldsymbol{\nabla}\cdot\boldsymbol{F}=0$; therefore the Jacobian determinant in (3.5) is equal to unity. A trajectory can be

stationary :	$\boldsymbol{\Phi}^t(\boldsymbol{x})=\boldsymbol{x}$	for all t
periodic :	$\boldsymbol{\Phi}^t(\boldsymbol{x})=\boldsymbol{\Phi}^{t+T}(\boldsymbol{x})$	for a given minimum period T
aperiodic :	$\boldsymbol{\Phi}^t(\boldsymbol{x})\neq\boldsymbol{\Phi}^\tau(\boldsymbol{x})$	for all $t\neq\tau$.

Stationary points are usually equilibrium points of the potential energy function. Periodic trajectories can be stable or unstable, giving rise to quasiperiodic or chaotic behaviour, respectively, of nearby aperiodic trajectories.

The starting point for the investigation of the degree of irregularity of a complex dynamical system is therefore the analysis of the phase-space structure (equilibrium points and periodic motions). This will give us a qualitative view of the main features at a given value of the Hamiltonian parameters (usually the total energy), i.e., it should reveal the presence of stability regions and chaos, and which domain of initial conditions will display chaotic or quasiperiodic behaviour as time evolves. A more quantitative characterization of the degree of chaos requires the calculation of global indicators such as Lyapunov exponents or different definitions of entropy [9].

In a two-degree-of-freedom system, the study of the phase-space structure usually begins with the analysis of the Poincaré surface of section. This is a mapping of the phase space obtained by means of keeping one of the dynamical variables (say a position) fixed at a constant value. Evolving a properly chosen set of initial conditions, whenever the dynamical variable reaches this value for a trajectory, the other position and the corresponding conjugate momentum are recorded, and this will be done for every trajectory of the initial ensemble. In terms of the flow the Poincaré map is defined as

$$\boldsymbol{x}_{n+1}=\boldsymbol{\Phi}(\boldsymbol{x}_n) \tag{3.6}$$

where $\boldsymbol{x}$ are the dynamical variables intrinsic to the surface of the section. Periodic motions are then seen as fixed points of the Poincaré map, $\boldsymbol{x}_n=\boldsymbol{\Phi}(\boldsymbol{x}_n)$. Quasiperiodic trajectories will give rise to regular islands and chaotic trajectories to randomly distributed points on the surface of section (see figure 2).

It is clear that local stability of periodic motions is an important issue. To characterize the stability of a trajectory, we study the evolution in time of small deviations $\delta\boldsymbol{x}$ from the

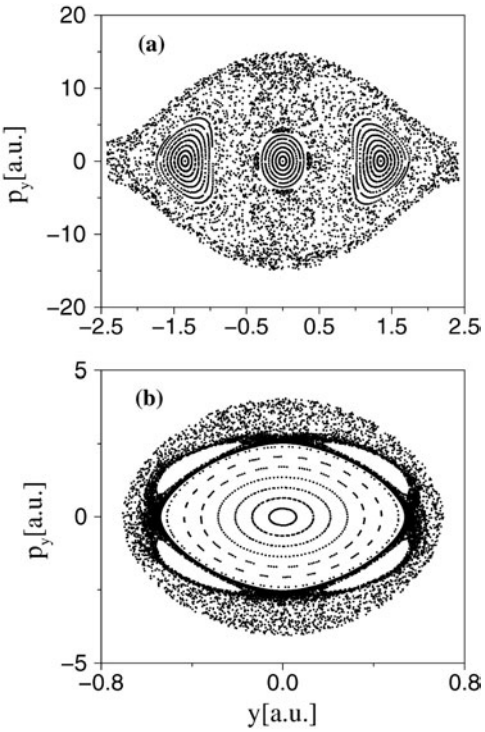

Figure 2. The Poincaré surface of section at a total energy of 80 meV, fixing the coordinate x: (*a*) $x_0 = 0$; (*b*) $x_0 = a/2$.

reference trajectory $\boldsymbol{x} = \boldsymbol{\Phi}^t(\boldsymbol{x}_0)$. On substituting the new trajectory $\boldsymbol{x}' = \boldsymbol{x} + \boldsymbol{\delta x}$ in (3.1) and expanding to linear order in $\boldsymbol{\delta x}$, we have that

$$\delta\dot{\boldsymbol{x}} = \partial_{\boldsymbol{x}}\boldsymbol{F}(\boldsymbol{x})\delta\boldsymbol{x}. \tag{3.7}$$

Since this is a system of linear equations, all of its solutions can be expressed as

$$\delta\boldsymbol{x}_t = \partial_{\boldsymbol{x}_0}\boldsymbol{\Phi}^t(\boldsymbol{x}_0)\cdot\delta\boldsymbol{x}_0 = \mathbf{M}(t,\boldsymbol{x}_0)\delta\boldsymbol{x}_0, \tag{3.8}$$

where $\mathbf{M}(t,\boldsymbol{x}_0)$ is the fundamental matrix, that also obeys the evolution equation

$$\dot{\mathbf{M}}(t,\boldsymbol{x}_0) = \partial_{\boldsymbol{x}_0}\boldsymbol{F}[\boldsymbol{\Phi}^t(\boldsymbol{x}_0)]\,\mathbf{M}(t,\boldsymbol{x}_0). \tag{3.9}$$

In this context it is called the *stability* matrix. If the trajectory $\boldsymbol{x}$ is periodic with period T, $\mathbf{M}(T,\boldsymbol{x}_0)$ is also known as the *monodromy* matrix. Its eigenvalues and eigenvectors determine the local behaviour of neighbouring trajectories, since they describe the deformation of the neighbourhood $\delta\boldsymbol{x}$ for a finite time t. Nearby trajectories can separate exponentially along *unstable* directions (given by the eigenvectors of the corresponding eigenvalues λ_i with $|\lambda_i| > 1$), approach each other along *stable* directions ($|\lambda_i| < 1$)), and maintain their distance along *marginal* directions ($|\lambda_i| = 1$).

In Hamiltonian systems, due to the symplectic structure of the Hamilton equations of motion, real eigenvalues come in pairs $(\lambda, 1/\lambda)$, one corresponding to the unstable direction and the other to the stable one, while complex eigenvalues come in pairs, $|\lambda| = 1$, or in quartets (only for systems with more than two degrees of freedom), $\lambda, 1/\lambda, \lambda^*, 1/\lambda^*$. For a two-dimensional Hamiltonian system, therefore, the Poincaré map first reduces the monodromy matrix to a 2×2 matrix. Then we can have a couple of real eigenvalues, which implies that our periodic orbit is unstable, or a pair of complex conjugated eigenvalues, implying that the periodic trajectory is stable.

All the analysis mentioned above refers to the properties of trajectories at a given value of the Hamiltonian parameters, say the total energy. However, one is frequently interested in obtaining information for a particular set or range of energies. In this case one has to study the parametric evolution of the phase-space structure. KAM theory (see, for example, [19]) gives a detailed understanding of the destruction of individual tori in phase space under perturbations. However, we would like to obtain a *global* picture of the phase-space structure at any relevant energy. A good strategy is to follow the evolution with energy of the principal periodic orbits. By 'principal' we mean the simplest ones (those with smaller periods and simplest topology in general), since periodic orbits of higher periods usually originate from them. An appropriate starting point for defining the main families of periodic orbits is Weinstein's theorem [22], that guarantees the existence, in the vicinity of an equilibrium point of the potential, of as many periodic orbits as degrees of freedom of the system. There are a number of numerical techniques for locating periodic orbits, even when they are highly unstable [23]. The one that we have used here is based on *shooting* methods for solving ordinary differential equations with two-point boundary conditions [24]. Then once we have located a given periodic orbit, for instance close to an equilibrium point, we change the energy slightly and find it again at the new total energy.

Let us express the eigenvalues of the monodromy matrix as $\lambda = \exp(\alpha T)$. For a two-dimensional Hamiltonian system and a periodic orbit of period 1 in the Poincaré map this matrix will take the form

$$\mathbf{M}_1 = \begin{pmatrix} \mathrm{e}^{\alpha_1} & 0 \\ 0 & \mathrm{e}^{-\alpha_1} \end{pmatrix}. \tag{3.10}$$

The stability of the periodic orbit can be deduced directly from the trace of the monodromy matrix. When the eigenvalues are complex, $\alpha_1 = \mathrm{i}\sigma_1$, we have that $\mathrm{Tr}\,\mathbf{M}_1 = 2\cos\sigma_1$. If they are real then $\mathrm{Tr}\,\mathbf{M}_1 = 2\cosh\alpha_1$. Therefore the stability is given by

$$|\mathrm{Tr}\,\mathbf{M}_1| \leqslant 2 \qquad \text{stable}$$
$$|\mathrm{Tr}\,\mathbf{M}_1| > 2 \qquad \text{unstable.}$$

For a periodic orbit which is a fixed point of period n of the Poincaré map, this criterion is equally valid on replacing $\mathbf{M}_1$ by $\mathbf{M}_n$.

To calculate the evolution of the monodromy matrix under the Poincaré map, we use the property $\mathbf{M}_n = \mathbf{M}_1^n$. Thus its trace after n iterations of the map will be

$$\mathrm{Tr}\,\mathbf{M}_n = 2\cos(n\sigma_1) = 2\cos\left[n\left\{\arccos\mathrm{Tr}\,\frac{\mathbf{M}_1}{2}\right\}\right] \tag{3.11}$$

for stable fixed points, and with the cosines replaced by hyperbolic cosines for unstable ones. Now the question is how periodic orbits appear in general. It is possible to show [25] that, when the stability matrix has an eigenvalue $\lambda = \pm 1$, the variational equations (3.9) have a periodic solution. Therefore a periodic orbit of period n in the Poincaré map can only appear (or one already existing disappear) when

$$\mathrm{Tr}\,\mathbf{M}_n = 2 \tag{3.12}$$

and this is called a *bifurcation*. Using (3.11), we can readily see that fixed points of higher periods n can be obtained from the period-1 fixed point whenever the relation

$$\mathrm{Tr}\,\mathbf{M}_1 = 2\cos\frac{2\pi m}{n} \tag{3.13}$$

is fulfilled, where m is an integer number such that the cosine is modulo π. Unstable periodic orbits do not bifurcate (do not give rise to new ones), but they can change their stability. The possible types of bifurcation in two-dimensional Hamiltonian systems number only five [26,27]

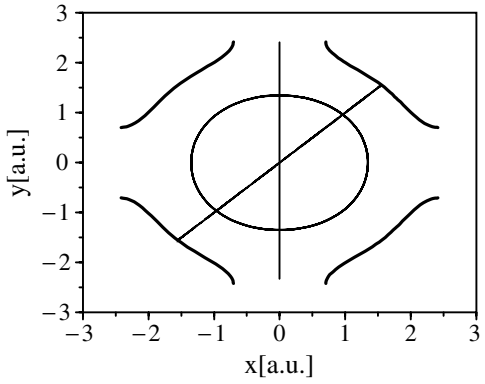

Figure 3. The main period-1 periodic orbits of the system at $E = 80$ meV restricted to the Wigner–Seitz cell (we show also the equipotential line at this energy).

but, for our purposes, the most important one is the period-doubling bifurcation ($n = 2, m = 1$, and $\mathrm{Tr}\,\mathbf{M}_1 = -2$) which changes the stability of the period-1 motion.

It is clear that locating the most important periodic orbits of period 1 and following the evolution of the monodromy matrix with energy, we can obtain a lot of information about how the phase-space structure changes through bifurcations. In the following section we will apply this theory to the deterministic dynamics of Na atoms in the Cu(001) potential previously described.

3.2. Phase-space structure for the Na/Cu(001) system

For an atom–surface interaction potential, the x- and y-coordinates extend from $-\infty$ to ∞ but, due to its periodicity, we can restrict the dynamics to the relevant Wigner–Seitz cell and impose periodic boundary conditions for the classical trajectories—that is, each time a trajectory crosses the boundary of a Wigner–Seitz cell we reinject it from the opposite boundary with the same momenta. Doing so, we get a dynamically significant picture of the phase space by fixing a coordinate for a Poincaré surface of section inside the appropriate Wigner–Seitz cell.

We found [28] three principal periodic motions arising from the minima of the potential wells at hollow sites. They are depicted for illustration in figure 3 at $E = 80$ meV (above the diffusion barrier along the x- and y-directions) restricted to the Wigner–Seitz cell. One is an orbit parallel to the x-direction or, equivalently, the y-direction (due to the symmetry of the potential, all periodic orbits with a reflection symmetry about the plane $x = 0$ have their counterpart in orbits with reflection symmetry about $y = 0$). For energies below the saddle-point barrier, $E_s \sim 74.6$ meV, this orbit represents a frustrated parallel translation, but for $E > E_s$ it describes free drifting motions along the x- or y-directions. Because the frequencies of these two modes are degenerate, they can be added or subtracted to give also two normal modes along the [100] or [010] azimuths (the diagonal directions). Note that the PES has also a reflection symmetry about the $x = y$ or $-y$ planes. This periodic orbit is localized for $E < 84.49$ meV and free above this energy. Finally, a circular-type orbit, analogous to a frustrated rotation, also starts from the hollow minimum. This orbit describes a localized motion inside the potential well even at energies greater than the on-top maxima, $E_{max} \sim 85.5$ meV, and it is responsible for the intrawell dynamics. We can understand the motion of the circular orbit at low energies as a combination of the frustrated translations along x and y with different phases, in analogy with the problem of normal modes of vibration [29]. The parallel and circular orbits are stable inside the well, but the diagonal one is unstable.

Close to the potential minima the system is nearly integrable, and information about the fundamental frequency of localized motions can be obtained by semiclassical quantization

of the parallel translations. The Einstein–Brillouin–Keller quantization condition can be expressed as [30]

$$\frac{1}{2\pi}\oint_C (p_x\,\mathrm{d}x + p_y\,\mathrm{d}y) = \hbar\left(n + \frac{\mu}{4}\right), \qquad n = 0, 1, 2, \ldots \tag{3.14}$$

where the action integrals are calculated along topologically independent closed paths defining a torus in phase space, and μ is the Maslov index which depends only on the topology of the classical orbit ($\mu = 2$ in our case). For the parallel translations, one of the momenta is always zero and the problem is reduced to one dimension; therefore the periodic orbit is semiclassically quantized by calculating its action integral along one period as we change the energy. When the quantization condition is matched for $n = 0$, this will give an estimate of the fundamental frequency from $\omega_0 = 2E/\hbar$. The value obtained is $\omega_0 = 6.4$ meV which agrees well with the experimentally determined frequency of the T mode [12] (6 meV). Note that by calculating energy differences at different values of n in (3.14), we could also obtain an estimate of the anharmonicity fitting the potential along the x- or y-directions to a first-order anharmonic expansion. Although experimental measurements of anharmonicity have not been reported for this problem, such simple models have been shown to work well for adsorption of CO on a Cu(001) surface [31].

For all of the three periodic motions, the trace of their monodromy matrices has been followed with change in energy in order to detect their bifurcations and changes of stability. This is shown in figure 4. For the circular orbit, figure 4(*a*), the opening of energetic barriers (indicated by arrows) does not seem to significantly affect its stability. Indeed, the orbit is quite stable (solid curve) until $E \sim 101$ meV where it suddenly undergoes a series of bifurcations of increasing periods. At $E > 101.6$ meV, $|\mathrm{Tr}\,\mathbf{M}_1| = 2$ and this orbit disappears or becomes very unstable. No more stable localized motions inside a potential well are visible at higher energies. This is intuitively expected, since localization is exclusively due to the effect of the potential wells and as we increase the energy the trajectories should follow straighter paths. However, it is interesting to see that at about 15 meV above E_{max}, localized motions are still stable.

For the straight motions along the x-, y-, or diagonal directions (figures 4(*b*) and (*c*), respectively), the opening of energetic barriers changes their character from localized to diffusing, although the topology of the orbit remains the same. For the motion along the $[1\bar{1}0]$ and [110] azimuths, the orbit is localized and stable until $E = E_s$, where it becomes a free drifting motion. This change in the PES leads to an *abrupt bifurcation* (marked with an arrow in figure 4(*b*)) and the sudden onset of an infinite sequence of periodic orbits of all periods as the trace of the stability matrix approaches the value 2 (see equation (3.13)). Diffusing orbits along the x- or y-directions with all possible periods are created. Because the main orbit remains stable, an island-around-island structure is expected in the Poincaré surface of section, shown in part in figure 5—that is, a hierarchy of island chains of increasing resonant frequencies. This will give rise to a self-similar hierarchy of nested *cantori* in phase space [11]. These objects, which have the same fractal structure of a Cantor set, were first described by Percival and Aubry [32, 33], and form partial barriers for the flux of trajectories through phase space. This means that a general chaotic trajectory will be trapped for long times around this hierarchy of cantori, which induce long jumps along x- and y-directions. After the transition region of abrupt bifurcation, the main orbit continues to be stable until $E = 89.7$ meV, where it suffers a period-doubling bifurcation. Between this energy and $E = 110$ meV it remains unstable, and no stable drifting motions are seen to occur in the Poincaré surface of section; see figure 6. Above 110 meV it again becomes stable and remains so, as expected from the approach to the integrable limit.

For the diagonal motion along the [100] azimuth (figure 4(*c*)) a similar situation is expected, the difference being that, due to the non-separability of the term for the potential

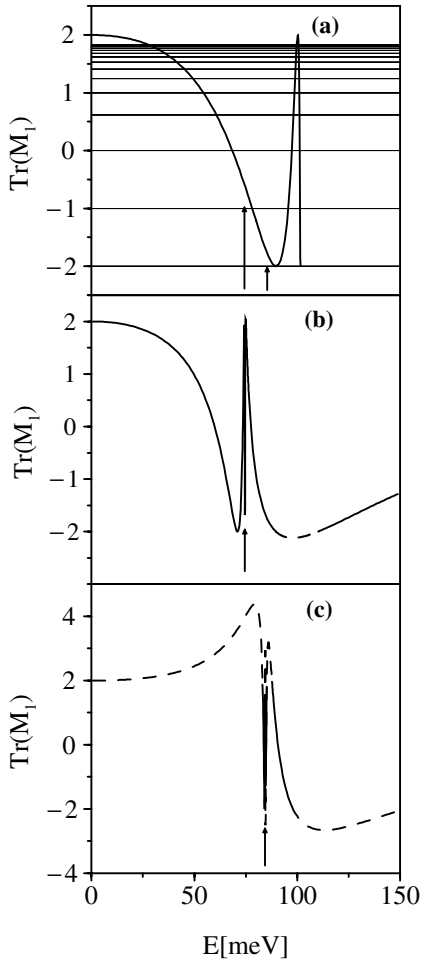

Figure 4. The trace of the stability matrix of the principal motions as a function of the energy. (*a*) Circular orbit. A sequence of bifurcations (from period doubling at $\mathrm{Tr}\,\mathbf{M} = -2$ up to period 15) are marked with solid thin lines. The arrows indicate the opening of energetic barriers ($E_s = 74.6$ and $E_{max} = 85.5$). (*b*) Parallel drifting motion. The energy of the saddle point along x or y, E_s, is marked with an arrow. (*c*) Diagonal diffusive motion. The arrow points to the energy of the on-top saddles at 84.49 meV. In all of them the stable orbits are plotted as solid curves and the unstable ones as dashed curves.

$V_2(x, y)$ around the minima, the motion is highly non-linear in the diagonal direction and the orbit is unstable. The interesting point is that, when the energetic barrier is open for this orbit to diffuse (at $E = 84.5$ meV), it coalesces with an orbit of the same topology originating at the small minima of the on-top sites and which in this case is stable. The abrupt bifurcation giving rise to drifting diagonal motions of all periods is seen again, and the main diagonal orbit is *stabilized* by the minima, so for 87.8 meV $\leqslant E \leqslant$ 97.5 meV it is stable, and then becomes unstable until, at $E > 150$ meV, it starts approaching the integrable limit. The stabilization of this diagonal motion will give rise to long jumps along the [100] and [010] azimuths, and this is consistent with the experimental observation that a high number of diffusing paths also exist along this direction, in addition to the paths across the saddle points along [110] or [1$\bar{1}$0] azimuths.

We note that inside the small potential wells at the on-top sites, the same three periodic motions described above are present, but now the parallel frustrated modes are unstable and the diagonal ones are stable. The rotational frustrated motion is also stable only for energies below the on-top maxima (between 82.74 and 85.51 meV). When this barrier is opened the motion turns unstable—opposite to what happened in the potential wells at the hollow sites. By semiclassically quantizing the (stable) diagonal periodic motion, we obtain a fundamental frequency $\omega_0^{top} \sim 2.4$ meV. Although for the present system the experimental results do not

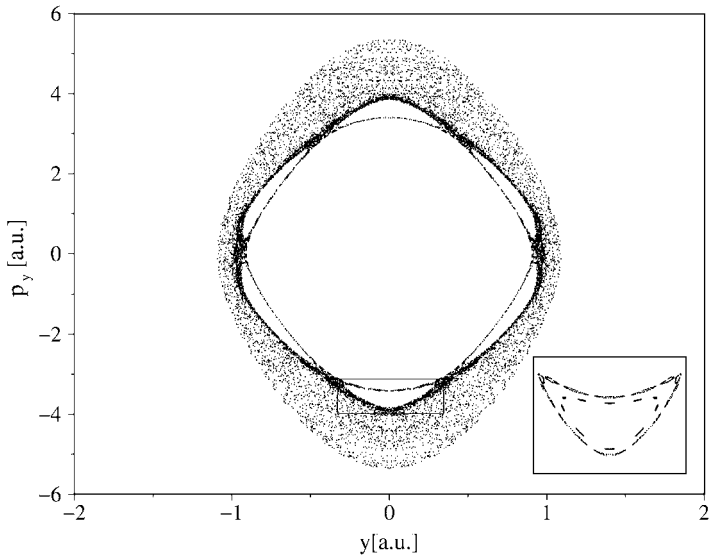

Figure 5. The Poincaré surface of section for $x = a/2$ and $E = 84$ meV, illustrating the island-around-island structure of the main parallel diffusing orbit. The inset shows some magnified island chains from the squared region.

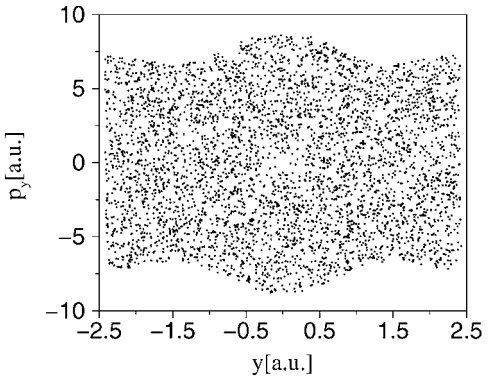

Figure 6. The Poincaré surface of section for $x_0 = a/2$ and $E = 100$ meV (no localized orbits can be shown when choosing this value of x_0 for the surface of section).

enable us to reach a conclusion about the existence of on-top site adsorption, it is intriguing to see that a weaker mode at approximately half the frequency of the T mode has been reported by Ellis and Toennies [13]. Indeed, there have been observations of stable on-top bound states for potassium on Cu(111) and Ni(111) [34].

4. Normal transport

In the previous section we briefly discussed how the classical dynamics can generate a probability density in phase space and thus could serve as a basis for the definition of statistical ensembles. The time evolution of the probability density is governed by the Liouville equation (3.4), while the evolution of a general dynamical variable A, which is a function of the phase-space point at any time, is given by an analogous equation [35]:

$$\frac{\partial}{\partial t}A(\boldsymbol{x}(t)) = -\hat{L}A(\boldsymbol{x}(t)), \tag{4.1}$$

where the Liouville operator is $\hat{L} = -\nabla(\boldsymbol{F}(\boldsymbol{x})\cdot\ )$. In order to obtain a macroscopic quantity as given from experiment, one should make a coarse graining in time, or a time average of the dynamical variable of interest, $\langle A\rangle = \lim_{\tau\to\infty}(1/\tau)\int_0^\tau A(\boldsymbol{x}(t))\,\mathrm{d}t$. When only the deterministic equations of motion are considered, it is the intrinsic dynamical instability or chaos that, under certain conditions, makes the time averages equivalent to phase-space averages (ergodic hypothesis) and justifies the calculation of thermodynamic properties, for instance, by molecular dynamics simulations [36]. However, when discussing transport properties, the relevant question is that of the decay of correlation functions with time, since the ordinary link between Liouvillian dynamics and transport coefficients is given by Green–Kubo relations. Ergodicity, though an important condition, is not very useful since no timescale can be defined using this property alone. Again, it is the dynamical instability which establishes intrinsic relaxation times of the correlation functions and allows one to obtain transport coefficients from it. Time correlation functions are also of experimental relevance since the spectra measured by various spectroscopic techniques are the power spectra of well-defined dynamical variables A.

Since the theory of transport processes, such as atomic surface diffusion, is very much related to the theory of stochastic processes and Brownian motion, here we will give a short account of it, emphasizing the main approximations that allow one to treat physical processes as stochastic processes. Then we will particularize the formalism to the case of diffusion of atoms on metal surfaces, and will establish a link between quantities that one can observe from experiments and those attainable from the chaotic dynamics, with application to the Na/Cu(001) system.

4.1. Generalities about Brownian motion

When discussing dynamics, both length scales and timescales need to be simultaneously considered. Typically wavelengths are compared with the mean free path, $\bar{l}$, and times with the mean collision time, τ_c. In this way, the dispersion (wavenumber–frequency) plane can be divided into three regions corresponding to the following three regimes: the hydrodynamic regime, $k\bar{l} \ll 1$, $\omega\tau_c \ll 1$; the kinetic regime, $k\bar{l} \sim 1$, $\omega\tau_c \sim 1$; and the free-particle regime, $k\bar{l} \gg 1$, $\omega\tau_c \gg 1$. In the first regime, macroscopic equations of motion of dynamical variables are required, whereas in the second regime, the microscopic level of equations of motion of such variables is studied. When we want to bridge between the microscopic and macroscopic worlds, we need first to clarify the relationship between the two types of dynamical variables. To this end, a 'coarse-graining' procedure has to be carried out. Thus, for example, the difference between the microscopic particle density and the hydrodynamic local density relies on the fact that the second is obtained by averaging the first over both a volume, which is macroscopically small but still sufficiently large to ensure that the relative fluctuation in the number of particles is negligible, and a time interval that is short on a macroscopic scale but long in comparison with τ_c. After that smoothing step is complete, the regression hypothesis due to Onsager [37], which can be justified on the basis of the linear response theory by means of the fluctuation-dissipation theorem [38], comes to nicely and linearly connect both worlds. In very simple words, such a hypothesis states that the relaxation of macroscopic systems not far from equilibrium is governed by the same laws as the regression of spontaneous microscopic fluctuations in an equilibrium system. This hypothesis provides, for example, a method for computing rate constants from microscopic laws. Once we have made such assumptions, we can formally start with the microscopic expressions for the transport coefficients in terms of the correlation functions, and then suppose that the correlation functions derived from the hydrodynamic equations are identical to those [35].

In a similar vein, the stochasticization or randomization of a general, physical process is carried out by some sort of coarse graining in space as well as in time. The degree of crudeness required by stochasticization is directly related to the degree of precision required for spatial and temporal measurements of dynamical variables. A stochastic physical process is called Markovian if its time evolution is determined by the present and not its past; it loses all memory of its past. As a consequence, Markovian laws of motion are differential equations which are first order with respect to time. Retardation effects and non-locality properties are then not taken into account. Furthermore, rate constants are defined in the Markov approximation within the master equation formalism but not in its generalized version where explicit memory functions are included. The paradigm of physical stochastic processes is the Brownian motion. The random-walk problem is often considered as a model for such a motion [39]. The Brownian motion is Markovian as well as Gaussian since the central-limit theorem applies for a sufficiently long time, at least greater than the correlation time of the system losing the memory of its initial conditions. If the number of particles is not too high and interactions between them can be ignored, Brownian particles are governed by the standard diffusion equation. The mean time, τ_c, between collisions of the Brownian particle and the surrounding medium has to be of the same order of magnitude or even slightly shorter than the average period of the fluctuating force in the surrounding medium.

A Brownian particle also satisfies a dynamical equation of the form (3.1), namely

$$\dot{\boldsymbol{x}} = \boldsymbol{u}(t) \tag{4.2}$$

where now the velocities $\boldsymbol{u}(t)$ and derived positions $\boldsymbol{x}$ are stochastic, rather than deterministic. Let us consider again a microscopic probability density $\rho(\boldsymbol{x}, t)$ giving the probability that the Brownian particle is at time t in the configuration-space volume $\mathrm{d}\boldsymbol{x}$. By invoking conservation of probability, the density $\rho(\boldsymbol{x}, t)$ is shown to obey a *stochastic* Liouville equation [40] of the form (3.4), namely

$$\partial_t \rho(\boldsymbol{x}, t) = \hat{L}\rho(\boldsymbol{x}, t) \tag{4.3}$$

where the differential operator $\hat{L} = -\boldsymbol{\nabla}\cdot[\boldsymbol{u}(t)\cdot]$ is a stochastic operator since $\boldsymbol{u}(t)$ is stochastic. In the reciprocal space, the above equation becomes

$$\partial_t \rho(\boldsymbol{k}, t) = -\mathrm{i}\boldsymbol{k}\cdot\boldsymbol{u}\rho(\boldsymbol{k}, t) \tag{4.4}$$

where $\rho(\boldsymbol{k}, t)$ is the Fourier transform of $\rho(\boldsymbol{x}, t)$. The solution of (4.4) for a given sample process $\boldsymbol{u}(t)$ is now

$$\rho(\boldsymbol{k}, t) = \rho(\boldsymbol{k}, 0)\exp\left[-\mathrm{i}\int_0^t \boldsymbol{k}\cdot\boldsymbol{u}(t')\,\mathrm{d}t'\right]. \tag{4.5}$$

Since $\boldsymbol{u}(t)$ is stochastic, we have to consider all the possibilities for it, and the probability distribution in Fourier space is given by averaging over all possible paths:

$$I(\boldsymbol{k}, t) = \langle\rho(\boldsymbol{k}, t)\rho(\boldsymbol{k}, 0)\rangle \propto \left\langle\exp\left(-\mathrm{i}\int_0^t \boldsymbol{k}\cdot\boldsymbol{u}(t')\,\mathrm{d}t'\right)\right\rangle. \tag{4.6}$$

This is the definition of the characteristic function for the stochastic variable $\boldsymbol{x}(t)$ [41]. Assuming that $\boldsymbol{x}(t)$ is Gaussian, the above equation can be expressed as [38]

$$I(\boldsymbol{k}, t) = \exp\left[-\boldsymbol{k}^2\langle u_k^2\rangle\int_0^t (t-\tau)\phi(\tau)\,\mathrm{d}\tau\right] \tag{4.7}$$

where $\phi(\tau)$ is the normalized velocity autocorrelation function and u_k stands for the velocity vector projected along $\boldsymbol{k}$. According to the discussion above, in order for the motion of the physical particle to behave as a Gaussian and Markovian process, a coarse graining in time

should be imposed, by taking the long-time limit. At long times, i.e., times longer than the mean collision time defined as

$$\tau_c = \int_0^\infty \phi(\tau)\,\mathrm{d}\tau, \tag{4.8}$$

equation (4.7) is approximated by

$$I(\boldsymbol{k}, t) \sim \exp[-k^2\langle u_{\boldsymbol{k}}^2\rangle\tau_c t + \delta] \tag{4.9}$$

with $\delta = k^2\int_0^\infty \tau\phi(\tau)\,\mathrm{d}\tau$. This function is the solution of the differential equation

$$\partial_t I(\boldsymbol{k}, t) = -\langle u_{\boldsymbol{k}}^2\rangle\tau_c k^2 I(\boldsymbol{k}, t), \tag{4.10}$$

that, on Fourier transforming back to real space, gives the standard diffusion equation

$$\partial_t P(\boldsymbol{x}, t) = D\,\nabla^2 P(\boldsymbol{x}, t) \tag{4.11}$$

with

$$D = \tau_c\langle u_{\boldsymbol{k}}^2\rangle \tag{4.12}$$

and $P(\boldsymbol{x}, t)$ the normalized autocorrelation function of the microscopic number density $\rho(\boldsymbol{x}, t)$ with the initial condition

$$P(\boldsymbol{x}, 0) = \delta(\boldsymbol{x} - \boldsymbol{x}_0). \tag{4.13}$$

4.2. Diffusion of adatoms on surfaces; scattering formalism

The theory behind QHAS experimental techniques is based on van Hove's formalism for quasielastic neutron scattering, for studying diffusion in the bulk [42]. This theory can be generalized to surface diffusion with some particularities. First, the substrate is usually assumed to be a perfect, periodic lattice. Second, adatoms are supposed to behave like Brownian particles. Third, diffusion is usually thermally activated, the diffusion barrier energy being a factor between 3 and 5 less than the binding energy and smaller than the thermal energy of adatoms; the hopping time is considered infinitesimally small. Fourth, the vibrational and diffusional motions of adsorbates are assumed to be decoupled although it is well known that vibrations can actually assist the diffusion process. And fifth, depending on the magnitude of the wavevectors involved, the lattice structure becomes important or not and different diffusion models can be conceived of. Thus, if only small wavenumbers are considered—that is, long wavelengths—a continuous diffusion model is applied. In contrast, at short wavelengths, jump diffusion models are used within the master equation formalism.

In analogy with the theory of liquids, the ensemble of diffusing classical particles on the surface is described by a time-dependent pair correlation function, $G(\boldsymbol{x}, t)$, whose Fourier transform in space and time, called the *dynamic structure factor*, is directly accessible by scattering experiments. This G-function, introduced originally by van Hove, is defined as the ensemble-averaged probability density of finding an adparticle at the surface position $\boldsymbol{x}$ at time t, given that an adparticle was at the origin at some arbitrary time $t = 0$. If the local adsorbate number density is given by $\rho(\boldsymbol{x}, t)$, then the normalized G-function or van Hove function can be expressed as

$$G(\boldsymbol{x}, t) = \frac{\langle\rho(\boldsymbol{x}, t)\rho(\boldsymbol{0}, 0)\rangle}{\langle\rho(\boldsymbol{x})\rangle}. \tag{4.14}$$

At low adparticle concentrations, when interactions between adsorbates can be ignored, such a function is only described by the so-called 'self'-part—that is, the dynamics for a single diffusing adparticle $G(\boldsymbol{x}, t) \equiv G_s(\boldsymbol{x}, t)$, and no ambiguity is introduced if the subscript s is

removed from now on. Strictly speaking, the G-function separates naturally into two terms called the 'self'-part and the 'distinct' part, the first being simpler to calculate than the second. Many efforts have been addressed to relating the two kinds of magnitude, the first one being the so-called convolution approximation due to Vineyard from 1958 [43]. Now it is clear that within classical mechanics, the time-dependent pair correlation self-function $G(\boldsymbol{x}, t)$ has the same physical meaning as the averaged probability density $P(\boldsymbol{x}, t)$ above, and when $\boldsymbol{x}(t)$ is considered as Gaussian it satisfies (4.7) with its spatial Fourier transform $I(\boldsymbol{k}, t)$, in this context known as the *intermediate-scattering function*.

As mentioned before, experimental information of the diffusing adparticles can be extracted from scattering experiments. Rather than neutron scattering, helium-atom scattering is preferred due to the fact that large cross sections (larger than in the gas phase) of adparticles are found although the experimental procedures are very similar. Additional advantages and disadvantages of this technique can be found elsewhere [3, 44].

There has been a great deal of argument about the requirements for the probe particles to provide unaffected time-dependent pair correlation functions. Generally speaking, the scattering particles should spend at least a time of order of the relaxation time of such correlation functions. In particular, it has been shown that He atoms from a room temperature source fulfil such requirements (velocities $<3 \times 10^3$ m s^{-1}). The quantity measured in the quasielastic experiment is the differential reflection probability (the probability of a projectile helium atom being scattered from the diffusing collective into a certain solid angle Ω with an energy exchange $\hbar\omega$) which is given by the following expression [3, 45]:

$$\frac{\mathrm{d}^2 R(\boldsymbol{K}, \omega)}{\mathrm{d}\Omega \, \mathrm{d}\omega} = n_d F^2 \int\int G(\boldsymbol{R}, t) \mathrm{e}^{\mathrm{i}(\boldsymbol{K}\cdot\boldsymbol{R} - \omega t)} \, \mathrm{d}\boldsymbol{R} \, \mathrm{d}t = n_d F^2 S(\boldsymbol{K}, \omega) \quad (4.15)$$

where $\boldsymbol{K}$ is the wavevector transfer parallel to the surface, $\boldsymbol{R}$ the coordinate parallel to the surface, n_d the diffusing particle concentration on the surface, and F the atomic form factor depending on the potential of the interaction between the projectiles and the adparticles. Scattering at small wavevector transfers provides information on large-distance correlations and, analogously, events with small energy transfers provide information on long-time correlations which contribute to the quasielastic intensity peak.

In the discussion so far on the diffusion process, no interaction potential between the substrate and the adsorbates has been considered. In other words, the diffusive motion is purely Brownian and is thought to be uncorrelated with the vibrational motion of the adsorbates. It is however well known that the former can be assisted by the latter. In principle, different length scales and timescales are involved in the two motions; vibrations are localized inside adsorption potential minima with high frequencies, and diffusion proceeds by jumping from one adsorption site to another between neighbours or even more distant ones. Obviously, under certain conditions, the two motions become more and more coupled. For example, temperatures higher than the diffusion barrier diminish the time spent by adatoms in an adsorption site and large friction coefficients can lead to jump distances of the order of the substrate lattice spacing. The work by Chen and Ying [13] can be considered as a first theoretical attempt to treat the two motions on an equal footing.

According to the above arguments, the dynamic structure factor in (4.15) will consist of several peaks: the quasielastic peak around $\omega = 0$ and several inelastic peaks due to adsorbate vibrations of low frequency, for the creation ($\omega < 0$) and annihilation ($\omega > 0$) events. Thus, if no correlation between the rapid motion due to vibrations and the slow diffusional motion exists, the G-function can be written as the convolution of the two contributions and therefore, by the convolution theorem, the total intermediate-scattering function will be the product of two Fourier transforms in space, one coming from vibration and the other from diffusion.

The total dynamic structure factor can then be expressed as the convolution in the frequency variable of the corresponding two dynamic structure factors. By considering the quasielastic (zero-phonon) and (one-phonon) inelastic contributions, the total dynamic structure factor can be expressed as a sum, each term coming from a decoupled motion. If the two motions are coupled (for example, by increasing the surface temperature), diffusion will be assisted by vibrations which will contribute to the quasielastic peak, and the corresponding sum is no longer valid. However, if the temperature is higher than the diffusion barrier, no detectable trace of vibrations is expected and only a broad quasielastic peak will be observed. The analysis of the line shape of the quasielastic peak is left to the next subsection.

4.3. Diffusional line shapes; sources of broadening

From an experimental point of view, natural line shapes corresponding to the smallest possible linewidths cannot be observed without special techniques because they are completely concealed by other broadening effects. Convolution techniques need to be applied. In damping processes, the existence of alternative relaxation channels shortens the lifetime of the corresponding process and therefore results in line broadening. In general, we have two types of broadening, homogeneous and inhomogeneous. The first one occurs when all the systems are in the same initial state and leads typically to Lorentzian line shapes. In contrast, the inhomogeneous broadening takes place when each system is in a different initial state, leading usually to Gaussian line shapes with a width many times greater than a Lorentzian one. This broadening consists of a superposition of many individual, homogeneous broadened lines which merge into a single broadened line. Globally, two kinds of relaxation are important: population and phase. Population decay constants are associated with the lifetimes of the system states—and the so-called dephasing constant is related to the process disturbing the phase of the wavefunction—but do not alter the population of the states. An anharmonic dephasing will occur when the surface temperature is comparable to the barrier height and, if it is much smaller, frictional coupling with substrate excitations becomes the dominant dephasing factor (anharmonic broadening).

As discussed in the preceding subsection, the relevant correlation function is the autocorrelation of the microscopic number density in reciprocal space, equation (4.6). According to the Wiener–Khintchine theorem, its power spectrum is given by

$$S(\boldsymbol{K},\omega)=\frac{1}{2\pi}\int_{-\infty}^{\infty}\mathrm{e}^{-\mathrm{i}\omega t}I(\boldsymbol{K},t)\,\mathrm{d}t \tag{4.16}$$

which is the dynamic structure factor. From the long-time approximation equation (4.9), a Lorentzian form for $S(\boldsymbol{K},\omega)$ is readily obtained:

$$S(\boldsymbol{K},\omega)\propto\frac{|\boldsymbol{K}|^2D}{\omega^2+|\boldsymbol{K}|^4D^2} \tag{4.17}$$

identifying D as in equation (4.12). Of course this form is also obtained by solving the ordinary diffusion equation (4.11) and then Fourier transforming in time and space.

It is interesting to consider the behaviour of the intermediate-scattering function $I(\boldsymbol{K},t)$ for the whole range of times [38]. According to the Doob's theorem, if a stationary process is Gaussian and Markovian, its correlation function decays exponentially in time. Thus the velocity autocorrelation function can be simply expressed as

$$\phi(\tau)=\mathrm{e}^{-t/\tau_c} \tag{4.18}$$

with τ_c the mean collision time, equation (4.8). Therefore the intermediate-scattering function given by equation (4.7) can be expressed as

$$I(\boldsymbol{K},t) = \exp\left[-\chi^2\left(\mathrm{e}^{-t/\tau_c} + \frac{t}{\tau_c} - 1\right)\right] \tag{4.19}$$

with

$$\chi = \tau_c\sqrt{\langle u^2\rangle}|\boldsymbol{K}| \equiv |\boldsymbol{K}|\bar{l} \tag{4.20}$$

a critical parameter governing, as we will see, the dynamical coherence of the diffusion process. Here $\bar{l}$ is the mean free path.

It is clear from a close inspection of equation (4.19) that, depending on the χ-values, the intermediate-scattering function can be approximated by different exponential functions. Thus, for example, when $\chi \to \infty$ or, equivalently, $\tau_c \to \infty$ or $\bar{l} \to \infty$, we obtain a Gaussian function (short-time approximation, $t \ll \tau_c$) as

$$I(\boldsymbol{K},t) \approx \mathrm{e}^{-\langle u^2\rangle|\boldsymbol{K}|^2t^2/4} \tag{4.21}$$

and the corresponding dynamic structure factor has a Gaussian shape:

$$S(\boldsymbol{K},\omega) \sim \frac{1}{|\boldsymbol{K}|u_0}\exp[-\omega^2/|\boldsymbol{K}|^2u_0^2] \tag{4.22}$$

with the mean velocity $u_0 = \sqrt{\langle u^2\rangle}$. The physical meaning of this is clear; one realizes that this corresponds to a van Hove function of the form

$$G(\boldsymbol{R},t) \sim \frac{1}{u_0t}\exp[-R^2/(t^2u_0^2)] \tag{4.23}$$

which is the probability for the particle to be displaced by $\boldsymbol{R}$ in a time t assuming a constant velocity $\boldsymbol{R}/t$ and an initial Maxwell–Boltzmann distribution of velocities, with $u_0 = \sqrt{2k_BT/m}$. This means that for times much shorter than the mean collision time, the particle behaves almost as if it is free, and dynamical coherence dominates.

In the opposite case, $\chi \ll 1$, we recover the long-time approximation (4.9) and the spectrum has the Lorentzian shape (4.17), with the obvious meaning that correlation among the different velocities is completely lost and the process is purely diffusive.

Fourier transformation of (4.19) for all ranges of time leads to Gamma and incomplete Gamma functions as follows:

$$S(\boldsymbol{K},\omega) = \frac{\tau_c\mathrm{e}^{\chi^2}}{\pi}\chi^{-2\chi^2}\left[\Gamma\left(\chi^2 + \mathrm{i}\frac{\omega}{\gamma}\right) - \Gamma\left(\chi^2 + \mathrm{i}\frac{\omega}{\gamma},\chi^2\right)\right] \tag{4.24}$$

where, as the value of the parameter χ decreases, the dynamic structure factor goes from a nearly Gaussian to a Lorentzian line shape and the spectrum becomes narrower and narrower. This effect is called motional narrowing [46]. Not only can the spectrum or dynamic structure factor as a whole be approximated by one of these shapes depending on the value of χ, but also—by the general property of the Fourier transform—we see that around $\omega = 0$, the behaviour of $S(\boldsymbol{K},\omega)$ is governed by the asymptotic behaviour of $\phi(t)$ for large t, and for large ω by that of $\phi(t)$ for small t. Therefore, the shape of the quasielastic peak at the centre will be close to Lorentzian while the wings are close to a Gaussian form. Alternatively, from an experimental point of view, what can also be varied is the magnitude of $\boldsymbol{K}$ through the initial conditions of the atomic beam (incident energy and angle) and therefore again the χ-value. Thus, a change of shape is observed when decreasing the $|\boldsymbol{K}|$ values. Moreover, when $|\boldsymbol{K}|$ is very large, we have another source of 'non-Lorentzianity', due to the fact that vibrations begin to play an important role in the diffusion process.

Finally, the true line shape observed has to be a convolution of the response function of the detector and the line shape (from Gaussian to Lorentzian) due to diffusional motion. In the long-time approximation, the resulting convolution function is called the Voigt profile.

4.4. The Langevin and Kramers equations; first-passage-time distribution

In order to consider the motion of the physical particle as a stochastic process, not only a coarse graining in time similar to the one performed to obtain equation (4.11) from (4.7), but also a coarse graining in space is necessary. This is naturally accounted for in the Langevin description of Brownian motion. The dynamical system of interest is usually characterized by a small number of degrees of freedom, while the reservoir or heat bath is a large, complex system with many (possibly an infinite number of) degrees of freedom. Then, the degrees of freedom of the reservoir are masked from observation by additional assumptions, basically that the relaxation or damping time governing the rate at which the dynamical system approaches equilibrium (steady state) with the reservoir is much larger than the reservoir fluctuation correlation time. Moreover, the interaction time is considered instantaneously short compared to the time of change of a given system property. Therefore the effect of the reservoir is only considered through a randomly fluctuating force which, according to the fluctuation-dissipation theorem, determines also the damping of the system due to friction. The equation of motion for the Brownian particle is then assumed to be

$$m\ddot{\boldsymbol{R}} = -\nabla_{\boldsymbol{R}} V(\boldsymbol{R}) - \eta\dot{\boldsymbol{R}} + \boldsymbol{F}_r(t) \tag{4.25}$$

where m is the mass of the adparticles, V the adiabatic adsorption potential, $\gamma = \eta/m$ the friction coefficient, and $\boldsymbol{F}_r$ a random fluctuating force with zero mean and delta correlated in time; that is,

$$\langle \boldsymbol{F}_r(t) \cdot \boldsymbol{F}_r(t') \rangle = 2m\gamma k_B T \delta(t - t'). \tag{4.26}$$

This force is also supposed to be uncorrelated with the velocity:

$$\langle \boldsymbol{F}_r(t) \cdot \dot{\boldsymbol{R}}(t') \rangle = 0. \tag{4.27}$$

A random force with the Dirac δ-correlation is called white noise since its spectral distribution is independent of the frequency. Otherwise, it is called coloured noise.

The rigorous theoretical basis for simplifying the equations of motion by removing the rapidly varying degrees of freedom of the environment is due to Zwanzig [47] and Mori [48], and it is known as the projection operator formalism. In atom–surface diffusion, this formalism can be equally well applied by considering the Hamiltonian for the phonon bath [49]. A Gaussian white noise then corresponds to dynamical incoherence of the surface phonons.

By solving the Langevin equation numerically, one can obtain the individual Brownian trajectories for the adparticles. The relevant correlation functions are calculated by averaging over stochastic paths and time. The dynamic structure factor can be calculated from equations (4.6) and (4.16). Other quantities of interest, also related to the diffusion coefficient, are the MSD given by the Einstein relation:

$$D = \lim_{t\to\infty} \frac{1}{4t} \langle |\boldsymbol{R}(t) - \boldsymbol{R}(0)|^2 \rangle, \tag{4.28}$$

and the velocity power spectrum

$$Z(\omega) = \int_{-\infty}^{\infty} \langle \boldsymbol{u}(t) \cdot \boldsymbol{u}(0) \rangle \mathrm{e}^{-\mathrm{i}\omega t}\, \mathrm{d}t \tag{4.29}$$

which gives D in the limit of small frequencies:

$$D = \tfrac{1}{2} Z(\omega = 0), \tag{4.30}$$

since when the diffusion is normal, $Z(\omega)$ converges to a finite value as $\omega \to 0$. We note also that the power spectrum is related to the dynamic structure factor by [35]

$$Z(\omega) = \omega^2 \lim_{\boldsymbol{K}\to 0} \frac{S(\boldsymbol{K}, \omega)}{K^2}. \tag{4.31}$$

When $\boldsymbol{K} \to 0$, $S(\boldsymbol{K}, \omega)$ is adequately described by the Lorentzian form (4.17) and, substituting in (4.31), we recover the previous equation (4.30).

As stated earlier, a totally equivalent and complementary approach to the Langevin treatment of diffusion problems is the FP formalism. The FP equation is just an equation of motion for the distribution function of fluctuating, continuous macroscopic variables. From distributions functions, any average value of macroscopic variables is easily obtained by integration. Such an equation is not restricted to systems near thermal equilibrium; it could even be applied to systems far from equilibrium. The Klein–Kramers or Kramers (KK) [5] as well as the Smoluchowski [50] equations are special forms of the FP equation. The former is an equation of motion for the distribution function in the position and velocity space, $W(\boldsymbol{R}, \boldsymbol{u}, t)$, which describes Brownian particles in an external field. The KK equation corresponding to the stochastic differential equation (4.25) has the form

$$\partial_t W = \sum_{i=1}^{2} [-\partial_{x_i} u_i + \partial_{u_i}(\gamma u_i + \partial_{x_i} V) + \gamma u_0^2 \, \partial^2_{u_i u_j}] W \tag{4.32}$$

with $\boldsymbol{R} = (x_1, x_2)$ and $\boldsymbol{u} = (u_1, u_2)$, $u_0 = \sqrt{2k_B T/m}$, the thermal velocity. Analytical and numerical methods for solving the KK as well as FP equations can be found elsewhere [50]. The stationary solution of this equation is the Boltzmann distribution as required by equilibrium statistical mechanics. For large damping constants, the KK equation reduces to the Smoluchowski equation represented only in the position space. The KK equation approach has also been applied to atom–surface diffusion problems by several groups using one- and two-dimensional periodic potentials [16, 51].

The first-passage time (FPT) is the time at which a stochastic variable first leaves a given domain [50]. The FPT variable is also a stochastic variable because depends on each realization. There is special interest in the first moment of the FPT, the mean first-passage-time (MFPT) value. The well-known Kramers result on reaction rates [5] (Arrhenius behaviour) is considered as the first application of the MFPT. Transition rates or attempt frequencies are just the inverses of escape times or MFPT.

4.5. Normal deterministic transport in the Na/Cu system

An analysis of the influence of the simplest periodic motions on the short-time dynamics has been carried out in section 3.2 through semiclassical quantization of the main periodic orbits. They gave us an estimation of the frustrated translational motion frequency extracted from the experimental dynamic structure factors. We will see how their stabilities affect the long-time dynamics, at energies above the saddle-point barrier of the potential—in particular, the asymptotics for MSDs and power spectra, which for the case of normal diffusion is directly related to the diffusion coefficient.

As was said before, one expects a usual diffusive behaviour if the phase space is sufficiently chaotic. At energies far away from the abrupt bifurcations suffered by the diagonal and parallel diffusive orbits, but still not so high that the trivial integrable limit is attained, we have instability of the main periodic drifting motions; see figures 4 and 6. This will happen for energies between 90 and 110 meV. A typical chaotic trajectory is depicted in figure 7 for very long times, showing a very similar behaviour to that of a usual random walk: short jumps between different unit cells separated by small localization periods inside a cell. That is, average jump lengths between sites and mean waiting times inside a site are finite. In figure 8 we show the power spectrum, equation (4.29), and the MSD, numerically calculated, propagating an ensemble of initial conditions (typically between 100 and 1000 trajectories) randomly chosen in the chaotic region of figure 6. We see that as $\omega \to 0$ it converges to the constant value $2D$, equation (4.30), while the MSD

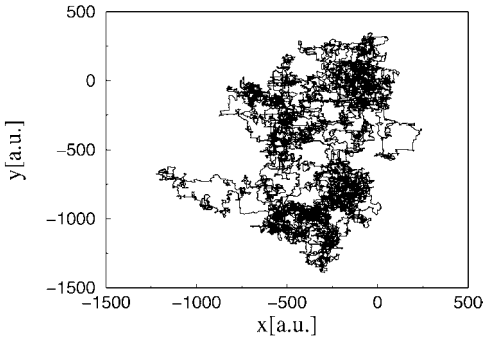

Figure 7. A chaotic trajectory at $E = 100$ meV run until $t \sim 20\,000$ ps (note the scales on the two axes; the length of the unit cell is $\sim 5a_0$).

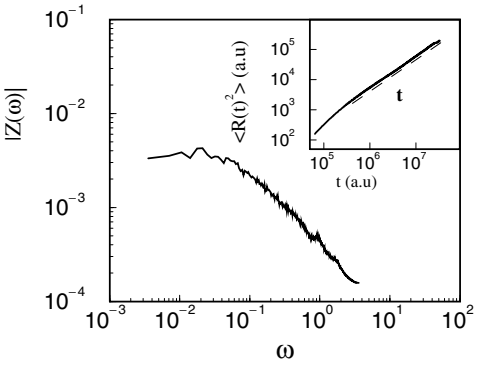

Figure 8. The velocity power spectrum at $E = 100$ meV. The frequency is given in units of the harmonic frequency $\omega_0 = 2\pi\sqrt{V_0/ma^2}$. Inset: the MSD at the same energy (also on a logarithmic scale).

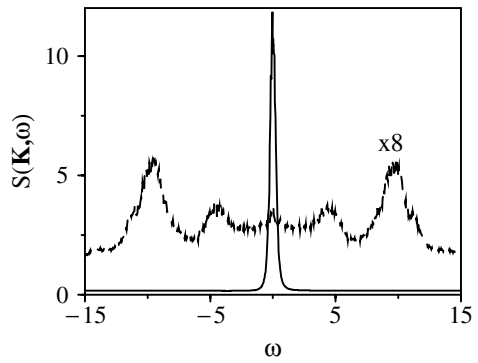

Figure 9. Dynamic structure factors obtained from a microcanonical ensemble of trajectories at $E = 100$ meV, using equations (4.6) and (4.16). Solid curve: $\boldsymbol{K} = 0.14$ Å^{-1}. Dashed curve magnified by 8.

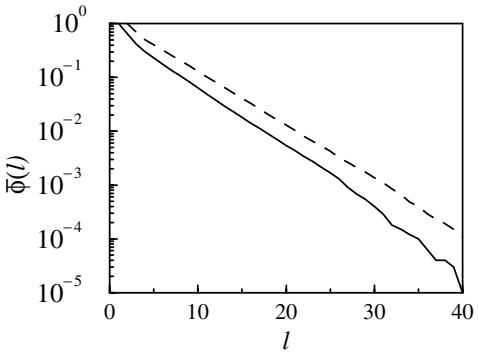

Figure 10. The integrated jump length distribution (solid curve) and the time-of-flight distribution (dashed curve) at $E = 100$ meV.

is linear in time according to the Einstein relation (4.28). The physical meaning of this is that the (deterministic) positions, or velocities, can be considered as Gaussian stochastic variables.

The analysis of the diffusional line shapes (quasielastic peak) of section 4.3 is also applicable to the dynamic structure factors obtained from the chaotic dynamics. In figure 9 we show $S(\boldsymbol{K}, \omega)$, equation (4.16), at two different values of the momentum transfer $\boldsymbol{K}$. At very small $\boldsymbol{K}$ (solid curve), we have a narrow quasielastic peak at $\omega = 0$ with a Lorentzian shape, due to the diffusional chaotic motion at long times and long mean free paths. At a value of $\boldsymbol{K}$ large enough that the maximum mean free path detected is less than one unit-cell length (dashed curve), no diffusional peak is observed, but instead the first and second inelastic excitations due to the adsorbate vibrations (T mode) are clearly visible. This could be a way to observe motional narrowing.

Let us now consider the distances along x- or y-directions travelled in a jump between different unit cells as a random variable, and calculate its distribution function $\phi(l)$. Jump length distributions are quantities of interest since they give an idea of the type of diffusing mechanism and friction regime [16, 51, 52], and sometimes they can be extracted from

experiment [18,53,54]. Moreover, they provide insight into the nature of the stochastic process, as we will see later. To numerically calculate jump length distributions in the Na/Cu system, we have used several methods and obtained equivalent results [28]. At energies below E_{max} (the on-top potential energy maxima), the potential barriers constrain the diffusive motion to the x- or y-directions, and we can define the beginning of a jump in x or y as when a trajectory crosses the activation barrier along one of these directions, the jump finishing when the momentum in this direction is reversed. Between two jumps, generally there is a waiting time inside a given unit cell where the trajectory executes chaotic motion and loses memory of the initial conditions; therefore two consecutive jumps are statistically independent. Note that, due to the symmetry of the PES, the jump distributions along x and y are identical. At higher energies, the particle can move freely along any direction and the criterion for the termination of a free jump is not so clear. We have found a more convenient way to count jumps: by calculating the Gaussian curvature at every integration step of a trajectory defined as

$$\kappa = \frac{|\dot{x}\ddot{y} - \ddot{x}\dot{y}|}{(\dot{x}^2 + \dot{y}^2)^{3/2}} \tag{4.33}$$

and the end (beginning) of a jump is considered to be the point of the trajectory where the radius of curvature, κ^{-1}, is less than some critical value chosen empirically.

The curvature criterion was proposed by Sholl and Skodje [55] in their investigation of Lévy flights in the Xe/Pt diffusion system. At energies below the top of the hill, for instance, we have found identical jump distributions $\phi(l)$ by using the first criterion of momentum change and the curvature criterion with the choice $\kappa^{-1} = 0.15\, a_0$.

To obtain good statistics it is better to calculate the integrated jump distribution [56] as

$$\bar{\phi}(l) = \int_l^\infty \phi(l')\, \mathrm{d}l' \tag{4.34}$$

and the corresponding $\phi(l)$ is obtained by differentiation of $\bar{\phi}(l)$. In figure 10 we present the integrated jump length probabilities (using as discrete jump length l, the number of unit cells traversed in the jump) for the normal diffusive regime, showing the typical exponential decay expected from the central-limit theorem (since the stochastic variable x, which can be considered as the sum of successive jumps, is Gaussian, the individual jump distributions ought to decay exponentially). The distribution of jump duration times considered as a random variable is also plotted as a dashed line, showing the same behaviour.

We have found numerically normal diffusive transport up to energies slightly above 120 meV. From figure 4, we see that the main parallel periodic orbit again becomes stable at $E \sim 110$ meV. The influence of this change of stability can be traced by relating the microcanonical diffusion coefficient to average jump lengths using some approximate statistical theories for the diffusion coefficient [28]. For instance, for extremely mobile adatoms we can use the kinetic theory of gases [2] to express the diffusion coefficient as

$$D(E) = \tfrac{1}{2}\langle u \rangle \bar{l} \tag{4.35}$$

where $\langle u \rangle$ is the average velocity and $\bar{l}$ is the mean free path. Correlations due to long flights are manifested as anomalous high values for $\bar{l}$. Another approximate expression for the microcanonical diffusion coefficient comes from the generalization of the simple random-walk picture to a random-flight formalism [39, 55] which in our case gives

$$D(E) = \tfrac{1}{2}\nu \langle l^2 \rangle \tag{4.36}$$

where ν is the frequency of flights and $\langle l^2 \rangle$ the average squared length of the jumps. The frequency ν can be computed as the total number of flights containing a non-zero number of barrier crossings, divided by the total time. This model assumes that successive flights are

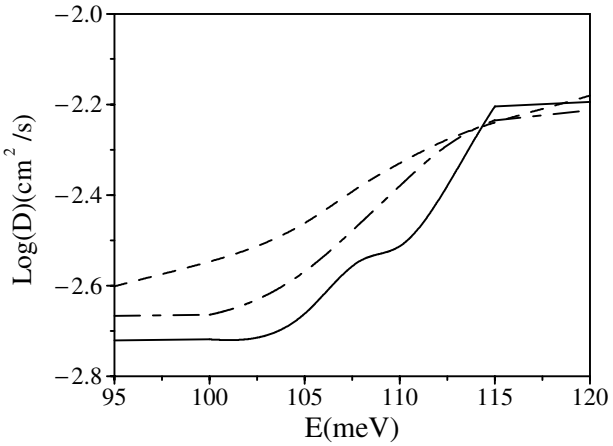

Figure 11. Microcanonical diffusion coefficients for an energy range between 95 and 120 meV. Solid curve: the exact diffusion coefficient from a fitting to the Einstein relations using microcanonical ensembles. Dashed curve: the approximation from the kinetic theory of gases equation (4.35). Dot–dashed curve: the random-flight approximation equation (4.36).

uncorrelated. If the jumps consist of only single hops, one should obviously have $\langle l^2 \rangle = a^2$. In figure 11 we plot the exact microcanonical diffusion coefficient obtained from molecular dynamics simulations using the Einstein formula (4.28) (or analogously (4.30)), versus the two approximations, equations (4.35) and (4.36). It is seen that around $E = 110$ meV the Einstein diffusion coefficient increases abruptly, due to the stabilization of the main parallel diffusing orbit. Although the two approximations used overestimate the diffusion coefficient at low energies, it is observed that the same qualitative feature is present in both models—that is, a more or less pronounced increase of the diffusion constant around 110 meV. In both approximations this is due to the increase in the jump length caused by the diffusing periodic orbit.

5. Anomalous transport

5.1. Description of anomalous diffusion

Transport processes of particles with MSDs violating Einstein's law for Brownian motion, equation (4.28), are generically called *anomalous diffusion* processes. This law is replaced by the more general form

$$\langle |\boldsymbol{x}(t) - \boldsymbol{x}(0)|^2 \rangle \sim D_\delta t^\delta \tag{5.1}$$

with $\delta < 1$ (subdiffusion) or $\delta > 1$ (enhanced diffusion or superdiffusion) describing diffusion processes slower or faster than ordinary Brownian motion. Anomalous diffusion has been known since Richardson's 1926 work [57] on turbulence (where he found $\delta = 3$ in (5.1)). Its study within transport theory of stochastic processes began in the late 1960s, promoted by the investigation of transport in amorphous semiconductors, a system where the traditional Brownian description of random walks failed [58]. Since then, experimental realizations of anomalous diffusion have been demonstrated for a large number of processes, among them transport of electrons in semiconductor microstructures [59], dynamics of polymeric systems [60], bacterial motion [61], rotating flows [62], and diffusion of adsorbed molecules at liquid–solid and liquid–liquid interfaces [63], to name just a few. A more extensive list of references can be found in a recent review [64].

Anomalous transport has been described within many different statistical frameworks. Simple (but with non-Brownian features) random-walk models accounted well for the first observations of anomalous diffusion [58, 65, 66]. These models also provide an intuitive physical picture of such a process: superdiffusion is originated by anomalously long jumps of a random walker (known as Lévy walks [67–69]) while subdiffusion can be associated with unusually long waiting times between successive walks [64, 70, 71]. Subdiffusive processes are usually modelled by a continuous-time random walk (CTRW) with a fractal distribution of waiting times, and therefore are also called 'fractal time' processes. In this review we will focus on *superdiffusion*, but we emphasize that both anomalous regimes can be described within the CTRW formalism [66, 72] and that the existence of Lévy or stable probability distributions [69, 73] is central to the explanation of general anomalous diffusion processes. We shall consider these models in detail in section 5.2. Additional statistical frameworks employed for the modelling of anomalous transport include Langevin equation approaches [74–78], FP equation description via fractional derivatives [64, 79, 80], and generalized thermostatistics [81, 82], as well as combined approaches.

Our next goal will be to identify deterministic diffusion mechanisms and to model them with simple random walkers, taking into account the information about the phase-space structure obtained from section 3. We will show that, when anomalous diffusion is present, the behaviour of some observable quantities such as velocity power spectra, dynamic structure factors, and mean first-passage times is significantly different from the normal diffusive case. In the rest of this section, we will particularize our treatment to a one-dimensional case in order to simplify the notation, but the relevant equations can be straightforwardly extended to higher dimensions.

5.2. Lévy walks and chaotic dynamics

From the results presented in section 4.5, it is clear that the chaotic dynamics can by itself mimic the behaviour of a stochastic system without the need to introduce any internal or external noise source. It has been widely shown that an unbound deterministic dynamical system with the ergodic property can be described by a usual diffusion equation [83] and thus can exhibit a normal diffusive behaviour. More interesting, because of its generality, is the case of a dynamical system with a mixed phase space—that is, with coexistence of regular and chaotic regions. Inside a chaotic region the ergodic property is expected to be approximately valid, but the existence of stability islands can subtly change the statistical properties of the system. In particular, the island structure can also induce anomalous transport under some circumstances.

Anomalous diffusion in two-dimensional Hamiltonian systems was studied some time ago in a model potential [56, 84]. There the existence of Lévy distributions of jump lengths was shown to be crucial for the explanation of this anomalous behaviour. We will apply the same analysis to the Na/Cu(001) system and exploit our knowledge of the phase-space structure to obtain a deeper insight on how Lévy walks appear in a non-separable periodic potential.

Lévy walks and Lévy flights are by now well established and widely used concepts in statistical physics [67]. The term Lévy *flight* is used to indicate a random walk in a continuous n-dimensional space displaying a stable or Lévy distribution of jump lengths and a finite average time between jumps. Due to the finiteness of the mean waiting times, this process is of Markovian nature. A general feature of Lévy distributions is that the MSD diverges:

$$\langle |x(t) - x(0)|^2 \rangle \to \infty \tag{5.2}$$

corresponding to the fact that long jumps are considered to be instantaneous. Clearly, for diffusion of a massive particle in physical space the velocity cannot be infinite; therefore these

unphysical flights are replaced by Lévy *walks* [70,85] in which one takes into account the time needed to complete each jump of the random walk. As a consequence, even when the average jump distance is infinite, the MSD after a time t will follow an algebraic dependence on time such as equation (5.1).

Now a word about Lévy distributions is in order: the theory of Brownian motion relies on the central-limit theorem, which roughly states that the sum of N independent and identically distributed random variables obeys a Gaussian distribution in the limit $N \to \infty$, *provided that the first and second moments do not diverge*. However, distributions which possess long, inverse-power-law tails have diverging second- and sometimes even first-order moments. A well-known example is the Cauchy distribution

$$p(x) = \frac{b}{\pi}\frac{1}{b^2 + x^2} \tag{5.3}$$

whose second-order moment is infinite. Nevertheless, Lévy, Khintchine, and other mathematicians developed the theory for these distributions in the 1930s [73] showing that a limiting distribution for the sum of x_n independent random variables exists if they are individually distributed according to

$$p(x) \sim \frac{\alpha b^\alpha c_\pm}{|x|^{1+\alpha}} \qquad \text{for } x \to \pm\infty \tag{5.4}$$

with $0 < \alpha < 2$ being the characteristic exponent; $b > 0$; $c_+ \geqslant 0$, $c_- \geqslant 0$ real constants; and where $\mathrm{Prob}(x < x_n < x + \mathrm{d}x) = p(x)\,\mathrm{d}x$. Moreover, the limiting distribution $L(x)$ for the sum $S_N = \sum_n x_n$, that is $\mathrm{Prob}(x < S_N < x + \mathrm{d}x) \overset{N\to\infty}{\longrightarrow} L(x)\,\mathrm{d}x$, is also a power law of the form

$$L(x) \sim \frac{A_{\alpha,\beta}}{|x|^{1+\alpha}} \tag{5.5}$$

where $A_{\alpha,\beta}$ is a constant depending on the characteristic exponent α and some asymmetry parameter β related to c_+ and c_-. This limiting Lévy or stable distribution has finite moments of order δ:

$$\langle |x|^\delta \rangle = \int_{-\infty}^{\infty} \mathrm{d}x\, |x|^\delta L(x) \qquad \text{if } 0 < \delta < \alpha. \tag{5.6}$$

From this we see that the variance does not exist if $\alpha < 2$ and that both the mean and the variance diverge if $\alpha < 1$. We also observe that the fact that the individual (5.4) and the limiting (5.5) distributions have identical forms implies some kind of self-similarity, or absence of scales.

An important result that we will use later is that Lévy distributions all have the same characteristic function which is of the form

$$L_{\alpha,\beta}(k) = \int_{-\infty}^{\infty} L(x)\mathrm{e}^{\mathrm{i}kx}\,\mathrm{d}x = \exp\left[\mathrm{i}\mu k - c|k|^\alpha\left(1 + \mathrm{i}\beta\frac{k}{|k|}\omega(k,a)\right)\right] \tag{5.7}$$

where μ is an arbitrary constant, $c \geqslant 0$ is a constant related to α, c_+, and c_-, and

$$\omega(k,\alpha) = \begin{cases} \tan(\pi\alpha/2) & \text{for } \alpha \neq 1 \\ (2/\pi)\ln|k| & \text{for } \alpha = 1. \end{cases} \tag{5.8}$$

These results constitute the Lévy–Gnedenko generalized central-limit theorem, and put long power-law-tailed distributions on the same level of importance as the well-known Gaussian distribution. In particular, for $\alpha = 2$, $\omega(k,\alpha) = 0$ and we recover the usual Gaussian distribution from equation (5.7). Note also that a symmetric ($\beta = 0$) $L_{\alpha,\beta}(k)$ with $\alpha = 1$ gives the Cauchy distribution, equation (5.3).

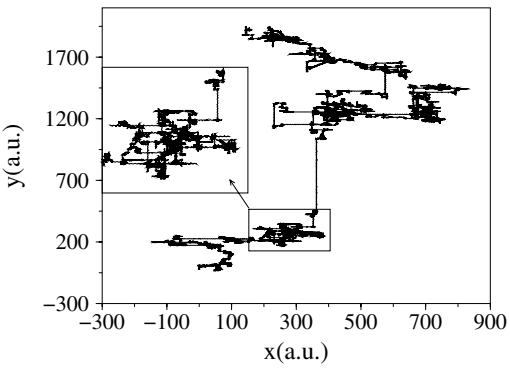

Figure 12. A chaotic trajectory at $E = 84$ meV, run until $t \sim 20\,000$ ps. Shown in the inset is an enlargement of the rectangular box.

In order to clarify why Lévy walks can be important for the statistical description of chaotic dynamics, let us recall the phase-space picture emerging from section 3.2. There we saw that, for energies between the saddle-point barrier along the x- and y-directions and a value slightly higher than the global maxima, there is a coexistence of stable periodic orbits of free-diffusive type and rotating ones, implying localization in a potential well. Now imagine a chaotic trajectory taken randomly from the stochastic region in figure 2. It is clear that, if it passes near one of the stability regions (left or right islands in figure 2(a)) of the circular orbit, it will spend some time inside the potential well performing a kind of rotating motion. On the other hand, if it gets close enough to the central chain of islands originated by the free-diffusive periodic orbit, it will have a large probability of making a long jump. Here we have the simplified picture of a random walker displaying long jumps between sites with a waiting time between them. The large-scale appearance of a typical chaotic trajectory is shown in figure 12 (note the scales on the x–y axes) together with an enlargement of a small region. The self-similar pattern exhibited in configuration space by these chaotic trajectories is evident (compare to figure 7 for the normal diffusion regime).

The important difference between localization around rotating orbits and free jumps can be predicted from the bifurcation diagrams shown in figure 4: while the translational motions suffer abrupt bifurcations producing an infinite hierarchy of islands and *cantori* in phase space, as sketched in figure 5, the trace of the monodromy matrix for the circular orbit changes smoothly with energy, which implies that at a given energy this hierarchy will be truncated. Therefore we expect a very high rate of long jumps between sites, while the waiting time statistics should give finite average times. This is the proper scenario for a random walker exhibiting *superdiffusion*, as has been shown in other systems [56]. Of course, if the island-around-island structure were due to localized periodic orbits, what one should expect is anomalously long waiting times and thus a subdiffusive regime, which is found in some Hamiltonian maps [68, 70]. We think that this deterministic mechanism for long jumps and superdiffusion, apart from specific details of this potential such as the coupling along the diagonal and the small maxima at the on-top sites, is generic for non-separable two-dimensional periodic potentials, since the ultimate reason for it is the abrupt bifurcation due to the opening of energetic barriers. Many adiabatic potentials for surface diffusion will present similar qualitative features.

The analytic description of anomalous diffusion in terms of random walks can be given following different models [65, 66, 69, 84, 86]. As we are interested in the connection between MSDs and velocity power spectra with Lévy statistics, we will use here the simplest models [65,66] containing the basic ingredients—that is, a walker that at random times follows statistically independent free paths of a given length, with the jump length following a Lévy distribution. Moreover, in order to ensure physical meaningfulness one should assume also

a duration time for each jump (a Lévy *walk*) and the simplest choice to make is that during the jump the walker has constant velocity. Geisel *et al* [65, 87] were the first to identify superdiffusion due to Lévy walks in chaotic Hamiltonian systems, and used this description within a *renewal* formalism [73,88] in which the central quantity is the probability distribution for a jump to be of duration t. This should be equal to the jump length distribution with the constant-velocity assumption; furthermore this distribution is considered to be of Lévy type (5.4). Expressing the autocorrelation function for the velocities in terms of the jump duration times distribution $\psi(t)$:

$$C(t) \sim \int_t^\infty (\tau - t)\psi(\tau)\,\mathrm{d}\tau, \tag{5.9}$$

and transforming to the Laplace domain, they extracted different behaviours for the power spectra and MSDs depending on the exponent α from $\psi(t) \sim t^{-1-\alpha}$.

Here we follow in detail an alternative approach, the CTRW approach, which leads to the same results but is more general in the sense that it can contain both the superdiffusive and subdiffusive regimes. It will also allow us to derive some important relations that we shall use later for other purposes. In the CTRW formalism [66, 84], the central quantity is $\psi(l, t)$, the probability density for moving a distance l at time t in a single motion event. As a simple picture, we can consider particles that move from site to site through single jumps, then stop and choose a new direction and time of sojourn at random, according to given probabilities. We see that not only jump distributions—as in the renewal formalism—but also *waiting time* distributions come into play. If jump lengths and waiting times are independent random variables, $\psi(l, t)$ can be written as

$$\psi(l, t) = \phi(l)w(t), \tag{5.10}$$

with $\phi(l)$ the probability for a jump to be of length l and $w(t)$ the probability for a waiting time in the interval $(t, t + \mathrm{d}t)$. Then we are led to the instantaneous jump picture (Lévy flights). In order to obtain Lévy walks and a duration time for the jumps, one can introduce a space-time coupling [66, 84, 86] and express $\psi(l, t)$ as

$$\psi(l, t) = p(l|t)\phi(l) \tag{5.11}$$

where $p(l|t)$ is the conditional probability of moving a distance l in a time t. Now one assumes a Lévy distribution for $\phi(l)$ as in (5.4), and jumps of constant velocity, i.e., $p(l|t) = \delta(t - |l|/v_0)$. The desired quantity is the pair correlation self-function $G(x, t)$ which we recall is the probability of being at position x at time t with initial condition $G(0, 0) = \delta(0)$. This is related to $\psi(x, t)$ in a standard way [86] by

$$G(x, t) = \sum_{x'} \int_0^t G(x', \tau)\psi(x - x', t - \tau)\,\mathrm{d}\tau + \Phi(t)\delta_{x,0}, \tag{5.12}$$

where

$$\Phi(t) = 1 - \int_0^t w(\tau)\,\mathrm{d}\tau \tag{5.13}$$

is the probability of survival at the initial site. The initial condition of starting from $x = 0$ at $t = 0$ is incorporated in the Kronecker delta (the x-variable is now discrete, since we assume that the particle is located only at active sites, separated by a distance a). The above relation is an integral equation that can be easily solved by Fourier–Laplace transformation $(x, t) \longrightarrow (K, s)$, since in the Fourier–Laplace domain it becomes

$$G(K, s) = G(K, s)\psi(K, s) + \Phi(s), \tag{5.14}$$

with the solution

$$G(K,s) = \frac{1-w(s)}{s}\frac{1}{1-\psi(K,s)}, \tag{5.15}$$

using the Laplace transform of (5.13), $\Phi(s) = [1-w(s)]/s$. Note that this is not the dynamic structure factor, since we have used Laplace transformation in time rather than Fourier transformation, but it can be easily generated from it. In fact, since the van Hove function $G(x,t)$ in (4.14) is an even function of time, the dynamic structure factor may be written as

$$S(K,\omega) = \frac{1}{\pi}\,\mathrm{Re}[G(K,\mathrm{i}\omega)]. \tag{5.16}$$

Now, using the expression

$$\psi(x,t) \sim x^{-1-\alpha}\delta(t - x/|v_0|) \tag{5.17}$$

in the CTRW with coupled memory, equation (5.11), one arrives at the following *asymptotic* expansions for $\psi(K,s)$ [86], valid in the limit $K \to 0$, $s \to 0$:

$$\psi(K,s) \sim 1 - \bar{\tau}s - CK^2 \qquad \alpha \geqslant 2 \tag{5.18}$$

$$\psi(K,s) \sim 1 - \bar{\tau}s - CK^2 s^{\alpha-2} \qquad 1 < \alpha < 2 \tag{5.19}$$

where $\bar{\tau} = \int \mathrm{d}t\, t \int \psi(x,t)\,\mathrm{d}x$ or mean waiting time is finite for $\alpha > 1$. Therefore the waiting time distribution has the asymptotic $s \to 0$ form, $w(s) \sim 1 - \bar{\tau}s$, for both α-regimes. Introducing the above equations into (5.15) one obtains for the Fourier–Laplace transform of the G-function

$$G(K,s) \sim \frac{1}{s + CK^2/\bar{\tau}} \qquad \alpha \geqslant 2 \tag{5.20}$$

$$G(K,s) \sim \frac{\bar{\tau}s^{2-\alpha}}{\bar{\tau}s^{3-\alpha} + CK^2} \qquad 1 < \alpha < 2. \tag{5.21}$$

From the expression for the G-function in the Fourier–Laplace domain, we can obtain quantities of interest. For instance, using the relation between the moments and the characteristic function [41]:

$$\langle x^2(t)\rangle = -\left.\frac{\partial I(K,t)}{\partial K^2}\right|_{K=0}, \tag{5.22}$$

the MSDs from equations (5.20) and (5.21) are given by

$$\langle x(t)^2\rangle \sim t \qquad \alpha \geqslant 2 \tag{5.23}$$

$$\langle x(t)^2\rangle \sim t^{3-\alpha} \qquad 1 < \alpha < 2, \tag{5.24}$$

which show how the normal and anomalous diffusion regimes arise from the value α of the Lévy distribution (5.4).

To check the validity of these statistical models we have calculated [28] the MSDs and jump length distributions as in section 4.5. As stated before, for energies close to the onset of abrupt bifurcations, between 75 and 90 meV, a kind of superdiffusive Lévy walk model is expected to describe the chaotic dynamics. In figure 13 we plot the MSD at two different energies, 84 and 80 meV; the plots show the anomalous diffusive behaviour, with $\alpha \sim 3/2$ and $\alpha \sim 5/4$ respectively, as taken from (5.24). The corresponding integrated jump length distributions are shown in figure 14, which clearly are of Lévy type (we also stress the fact that the power-law behaviour is expected for *long* jump lengths), with exponents in agreement with those of the MSD following (5.24). To observe superdiffusion, in addition to the Lévy jump length probability, one must have waiting time distributions of Gaussian type, or decaying faster than the sojourn times. In figure 15 we show the first-passage-time distribution through the interval $-a/2 \leqslant x \leqslant a/2$ (a is the unit-cell length), at $E = 80$ meV, of an initial ensemble of trajectories started along the line $x(0) = 0$. The decaying is exponential, implying that the mean waiting time inside a unit cell is finite.

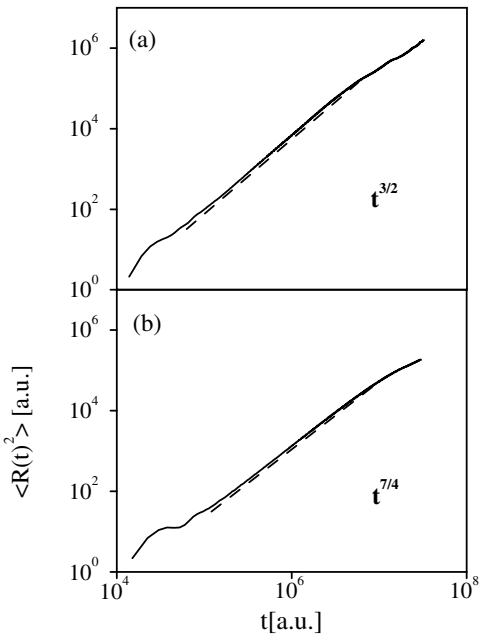

Figure 13. pt(a) The MSD at $E = 80$ meV; (*b*) the MSD at $E = 84$ meV. Note the logarithmic scales on both axes.

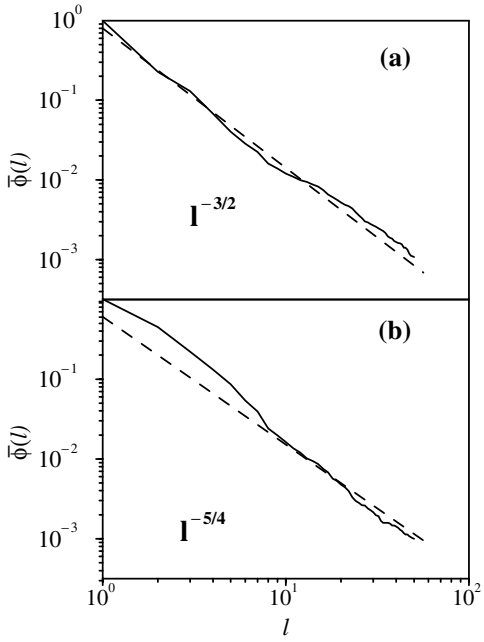

Figure 14. Integrated jump probability distributions (solid curves) at (*a*) $E = 84$ meV and (*b*) $E = 80$ meV. Only jumps with lengths less than 50 unit cells are shown. The theoretical predictions given by equation (5.4) are plotted as dashed curves.

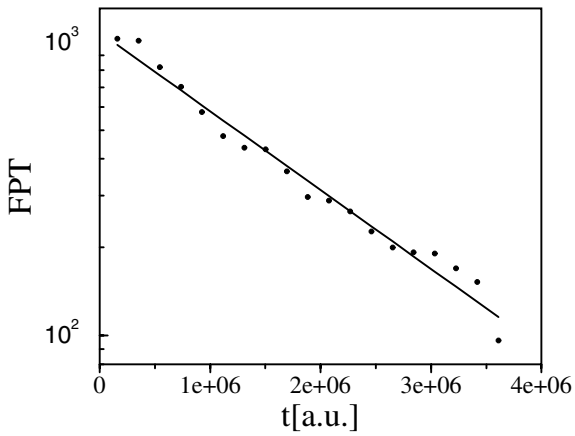

Figure 15. The first-passage-time distribution through one unit-cell boundary ($x = \pm a/2$) for an initial ensemble of chaotic trajectories with $x(0) = 0$.

5.3. Power spectra and dynamic structure factors

A quantity where it is convenient to observe anomalous diffusive behaviour, because it can be related to experiment, is the velocity power spectrum. At very small frequencies the power spectrum contains information on the diffusional dynamics at long times (indeed, for normal diffusion it gives the diffusion coefficient at $\omega = 0$; see (4.30) and figure 8), and from it

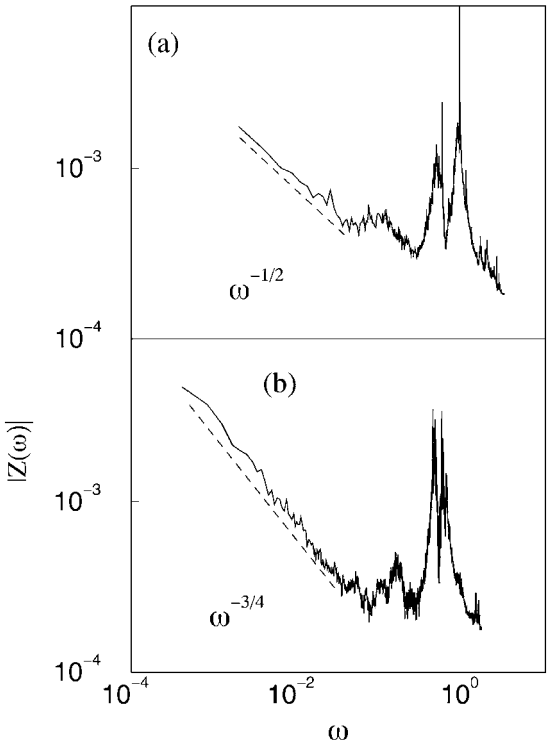

Figure 16. Velocity power spectra at two different energies: (*a*) $E = 84$ meV and (*b*) $E = 80$ meV. The frequencies are given in units of the harmonic frequency $\omega_0 = 2\pi\sqrt{V_0/ma^2}$.

the behaviour of MSDs and the structure factor can be extracted. At long times, the velocity autocorrelation function and MSD satisfy the Green–Kubo relationship [35]:

$$\sigma^2(t) \equiv \langle x^2(t)\rangle \sim 2t \int_0^t \langle v(0)v(\tau)\rangle \, \mathrm{d}\tau, \tag{5.25}$$

valid if the velocity is a Markov process. Performing the Laplace transformation, one obtains the relation

$$\sigma^2(s) = -\frac{1}{s}\frac{\partial}{\partial s}Z(s) + \frac{Z(s)}{s^2} \tag{5.26}$$

where $Z(s)$ is the Laplace transform of the velocity autocorrelation function. Now, if we have an anomalous behaviour of the MSD $\sigma^2(t)$ as given by equation (5.24), this implies, substituting in the above equation (5.26) and using the relationship between Laplace and Fourier transforms, that the power spectrum, equation (4.29), should behave at small frequencies as

$$Z(\omega) \sim \omega^{\alpha-2}. \tag{5.27}$$

Therefore, because $1 < \alpha < 2$, $Z(\omega)$ diverges at small frequencies, and the diffusion coefficient as defined by the Einstein relation or equivalently as in equation (4.30) does not exist. The behaviour of the velocity power spectrum at small frequencies is exemplified in figure 16, showing an exponent α in agreement with the one obtained from the MSD in figure 13; see also (5.24)–(5.27).

On the other hand, at large frequencies, the velocity power spectrum contains dynamical information on the short-time dynamics, and it is possible to extract from it the frequency of

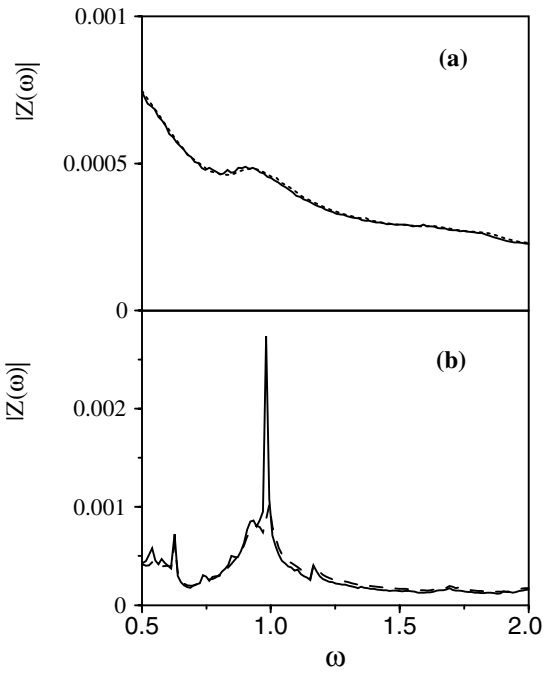

Figure 17. (*a*) The power spectrum at frequencies around ω_0 for $E = 100$ meV (normal diffusion regime) fitted with Padé approximants to show the structure of dynamical Pollicott–Ruelle resonances; (*b*) the power spectrum at finite frequencies for $E = 84$ meV (anomalous diffusion regime).

the frustrated translational mode [16,51]. When the deterministic dynamics is the relevant one, peaks in the power spectrum at finite frequencies can be associated with resonances (poles of the power spectrum analytically continued in the imaginary plane [9,89,90]) which are related to the different modes of relaxation towards equilibrium governed by the classical dynamics. These are usually called Pollicott–Ruelle resonances. As an illustration, we present in figure 17 the finite-frequency spectra at $E = 100$ and 84 meV. The dashed curves are numerical Padé approximations used to extract the relevant poles. It is seen than when the system is closer to ergodicity (figure 17(*a*)) the peaks are much broader and we can discern only a single peak at $\omega = \omega_0$ which corresponds to the frequency of the frustrated translation. On the other hand, a richer structure of resonances can be seen in the case of anomalous diffusion, figure 17(*b*), which is the hallmark of different stable periodic orbits. Here we merely mention that real poles of the analytically continued power spectrum give purely decaying behaviour for the velocity autocorrelation function (or the autocorrelation function of any observable in general), while complex poles represent damped oscillations with the real part giving the period of the oscillation and the imaginary part the relaxation rate [9,90].

The existence of stable or Lévy distributions of the type (5.4) affects the wavevector-transfer or K-dependence of the dynamic structure factor. To see this, suppose a one-dimensional random walker to have the algebraic jump length probability distribution (5.4) for the individual steps (a simple model is the Weierstrass random walk [69, 91, 92]). Then, the probability density for the walker being at position x after N steps, these being independent, is the convolution

$$G_N(x) = \phi(l) * \cdots * \phi(l), \tag{5.28}$$

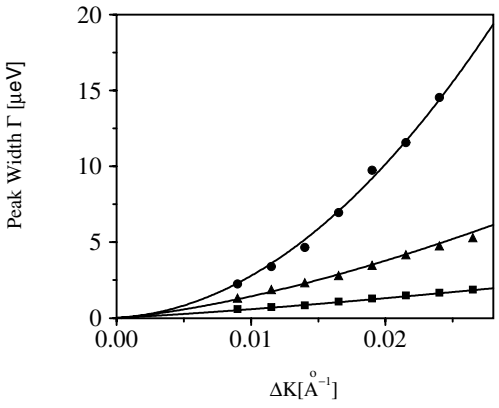

Figure 18. The FWHM of the dynamic structure factor at small parallel wavevector transfer K, for different energies. Circles: $E = 100$ meV, normal diffusion regime. Triangles: $E = 84$ meV. Squares: $E = 80$ meV. The solid curves show a fitting to the K-dependence given by equation (5.31).

N times, and where, by definition, $G_N(x)$ is a discrete time one-dimensional pair correlation function. In Fourier space, the intermediate-scattering function can then be expressed as

$$I_N(K) = \phi(K)^N. \tag{5.29}$$

For the probability distribution (5.4), the characteristic function $\phi(K)$ has the limiting $K \to 0$ form [69] (see also (5.7)):

$$\phi(K) = \mathrm{e}^{-c(\alpha)|Ka|^\alpha} \tag{5.30}$$

where a is the unit-cell length. By defining the time $t = N\Delta t$ and a generalized diffusion coefficient as $\mathcal{D} = c(\alpha)\lim_{a,\Delta t\to 0}(a^\alpha/\Delta t)$, and using equation (4.16), one readily finds for the dynamic structure factor at small K the functional form

$$S_s(K,\omega) = \frac{1}{\pi}\frac{\mathcal{D}K^\alpha}{\omega^2 + \mathcal{D}^2K^{2\alpha}}. \tag{5.31}$$

Note that within this Weierstrass random-walk approach, when $\alpha = 2$ the characteristic function (5.30) is a Gaussian and we recover the result for normal diffusion, equation (4.17). The prediction for the small-K behaviour of the dynamic structure factor (5.31) is verified in figure 18. The FWHM of the numerically calculated $S_s(K,\omega)$ at different energies in the anomalous diffusion regime ($E = 80$ and 84 meV) are well fitted by the expression $\mathcal{D}K^\alpha$. The normal diffusion regime $\alpha = 2$ is also shown for comparison.

The above discussion entails taking the $K \to 0$ (or $x \to \infty$) limit for the two cases of normal and superdiffusive regimes. In order to relate the K-behaviour of the full width at half-maximum (FWHM) of the dynamic structure factor to jump length distributions, for all K in the range of the reciprocal lattice, one usually assumes a jump diffusion model [53, 93] and a master equation for $G(x,t)$. Working again with only one dimension, and discrete lattice sites x_i, the master equation reads

$$\frac{\partial G(x_i,t)}{\partial t} = \sum_{j\neq i}[W(x_i|x_j,t)G(x_j,t) - W(x_j|x_i,t)G(x_i,t)] \tag{5.32}$$

where $W(x_i|x_j,t) = \lim_{\Delta t\to 0} = p(x_i, t+\Delta t|x_j,t)/\Delta t$ is the probability of transition from site j to site i at time t, and of course $p(x_i,t|x_j,t')$ is the conditional probability of being at site i at time t given that it was at site j at time t'. Now the assumption is to consider time-independent transition probabilities, or transition probabilities per unit time $W(x_i|x_j)$, so that (5.32) can be solved by Fourier transforming in space [53] yielding

$$I(K,t) = \mathrm{e}^{-t/\tau(K)}I(K,0), \tag{5.33}$$

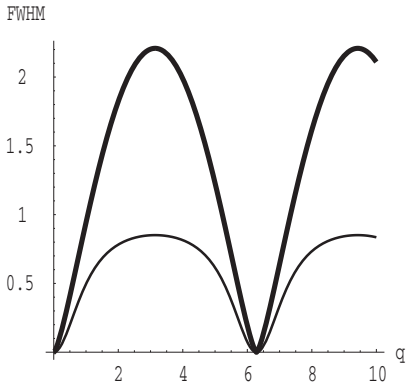

Figure 19. The FWHM of the structure factor from a jump diffusion model equation (5.36), in the normal diffusion regime (thick solid curve) and the anomalous diffusion regime (thin solid curve). Here $q = aK$. The parameters chosen have been $b = 1$ in equation (5.37) and $\alpha = 1.5$ in (5.38).

with $I(K,t) = \sum_i \exp(-\mathrm{i}Kx_i)G(x_i,t)$ the intermediate-scattering function, and

$$\tau^{-1}(K) = 2\sum_{j\neq i} W(x_j|x_i)\sin^2[K(x_j - x_i)/2]. \tag{5.34}$$

the inverse of the relaxation time. Now, because only differences in position appear in equation (5.34) and $x_j - x_i = la$, l being a positive integer and a the distance between adjacent sites, we can write

$$\tau^{-1}(K) = 2\nu\sum_{l=1}^{\infty} p(l)[1 - \cos(laK)], \tag{5.35}$$

where $p(l)$ is the jump distribution, or probability of jumping over l sites in a single jump, and ν the total jump rate, or probability of making a jump per unit time, $\nu = \sum_{i\neq j} W(x_j|x_i)$.

On Fourier transforming in time to obtain the dynamic structure factor, a Lorentzian shape with the FWHM given by

$$\Gamma = \tau^{-1}(K)/2 = \frac{\nu}{2}\sum_{l=1}^{\infty} p(l)[1 - \cos(laK)] \tag{5.36}$$

is again obtained. This expression is customarily used to obtain jump length probabilities from experimental or theoretical knowledge of the dynamic structure factor at different K, assuming normal diffusion. Here we show the different K-dependences of the FWHM in the case of superdiffusion. For normal diffusion, we saw that jump probabilities are distributed according to an exponential function, $p(l) \sim \mathrm{e}^{-bl}$, b being a positive constant. The FWHM can now be expressed in analytical form as

$$\Gamma = \frac{\nu(1 + \mathrm{e}^b)(1 + \cos(aK))}{4(\mathrm{e}^b - 1)(\cosh b + \cos(aK))}, \tag{5.37}$$

where the periodicity of the FWHM in the Bravais lattice is clear (see figure 19). For anomalous diffusion, we assume a Lévy distribution of jump lengths of the type (5.4), and the following expression for the FWHM is calculated:

$$\Gamma = \frac{\nu}{4}[2\xi(1+\alpha) - \mathrm{Li}_{1+\alpha}(\mathrm{e}^{-\mathrm{i}aK}) - \mathrm{Li}_{1+\alpha}(\mathrm{e}^{\mathrm{i}aK})]. \tag{5.38}$$

Here ξ is the Riemann zeta-function [94] and $\mathrm{Li}_n(z) = \sum_{k=1}^{\infty} z^k/k^n$ are the polylogarithmic or Jonquiére functions. In figure 19 we plot the FWHM for the case of anomalous diffusion with a Lévy exponent of $\alpha = 1.5$ (the deterministic case at $E = 84$ meV), and compare it with the case of normal diffusion to stress the differences.

5.4. Fractional dynamics

The divergence of second-order moments and the absence of a Gaussian distribution for the G-function imply that the usual diffusion equation (4.11) is no longer valid.

Here we see that a natural generalization of this equation for superdiffusion, assuming the existence of Lévy distributions of jump lengths, is given by a diffusion law with fractional derivatives in *space*. We will follow the derivation of reference [95]. Fractional derivatives in space are conveniently defined through the Riesz/Weyl fractional operator ∇^β [96], which has a simple form when one computes its Fourier transform, namely

$$\nabla^\beta f(K) = -|K|^\beta f(K) \tag{5.39}$$

leading in one dimension to the definition

$$\nabla^\beta = \frac{\partial^\beta}{\partial x^\beta} = -\frac{1}{2\pi}\int_{-\infty}^{+\infty} \mathrm{d}K\, \mathrm{e}^{-\mathrm{i}Kx}|K|^\beta. \tag{5.40}$$

Now, it has been shown that the integral equation for $G(x,t)$ in equation (5.12) is equivalent [86] to the following generalized master equation:

$$\frac{\partial}{\partial t}G(x,t) = \sum_{x'}\int_0^t W(x-x',t-\tau)G(x',\tau)\,\mathrm{d}\tau, \tag{5.41}$$

with the kernel (transition probability) in Fourier–Laplace space *defined* by

$$W(K,s) = \frac{\psi(K,s)-w(s)}{1-w(s)}s \tag{5.42}$$

where the functions $w(t)$ and $\psi(x,t)$ are the same as in section 5.2. Using a CTRW model with *uncoupled* jump length and waiting time distributions as in (5.10), where $\phi(x)$ is of Lévy type, leads to a limiting $(K,s)\to(0,0)$ distribution for $\psi(K,s)$ of the form

$$\psi(K,s) \sim 1 - \bar{\tau}s - CK^\alpha \tag{5.43}$$

which comes from expanding $\phi(K)$ and $w(s)$ in Taylor series and taking the small-t and small-K limits. Introducing this into the kernel yields

$$W(K,s) \sim -\frac{C}{\bar{\tau}}K^\alpha. \tag{5.44}$$

Considering as characteristic of the diffusion process only the limiting kernel of the diffusion process in the generalized master equation (5.41), and transforming it to Fourier–Laplace space, one obtains

$$sG(K,s) - G(K,0) = -\frac{C}{\bar{\tau}}K^\alpha G(K,s). \tag{5.45}$$

Upon inverting the transforms and using the definitions of the Riesz fractional operator (5.39)–(5.40), one obtains the *fractional* diffusion equation

$$\frac{\partial}{\partial t}G(x,t) = D_{eff}\frac{\partial^\alpha}{\partial x^\alpha}G(x,t), \tag{5.46}$$

where the effective diffusion constant is $D_{eff} = C/2\bar{\tau}$.

We note that this equation is linear in time, since Lévy flights with finite mean waiting times are Markovian. Corresponding equations for the subdiffusive regime have been derived [64,95] which have a fractional dependence on the *time* derivatives, since fractal time processes are not Markovian. We note also that the above fractional equation has as a solution for the characteristic function, when transformed to K-space, $I(K,t) = \exp[-D_{eff}t|K|^\alpha]$, which corresponds to a continuous Weierstrass random walk as given by (5.29)–(5.30) and leads to a dynamic structure factor of the form (5.31).

Fractional equations for anomalous superdiffusion have been generalized to include external force fields [97]

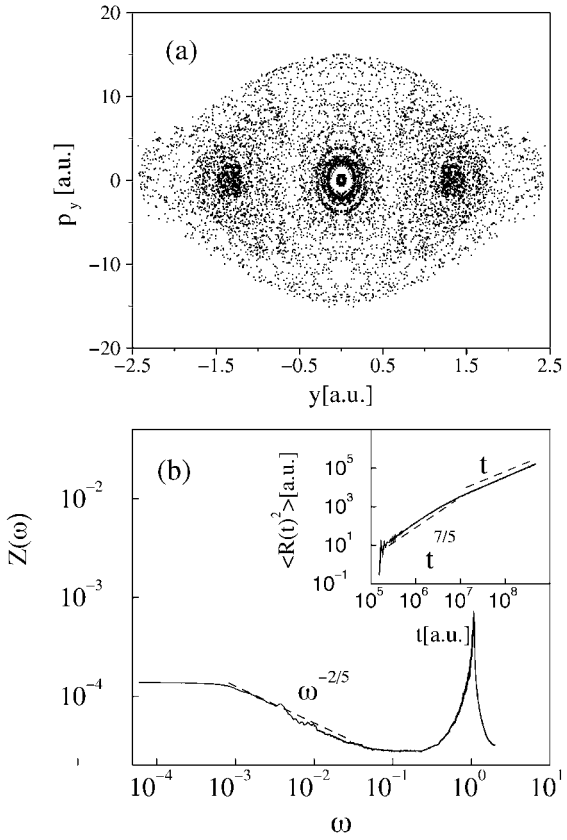

Figure 20. (*a*) The Poincaré surface of section at $x = 0$ of the full Langevin dynamics, equation (4.25), at $T = 50$ K and $\gamma = 10^{-3}$ ps^{-1}. (*b*) The velocity power spectrum and MSD (inset) for an ensemble of 1000 trajectories with a Maxwell distribution of velocities at the same temperature. The frequencies are in units of the fundamental frequency ω_0.

5.5. Influence of Gaussian white noise

The assumption that the system is in thermal equilibrium and that the dissipation mechanism is of the form $-\gamma \dot{\boldsymbol{R}}$ defines the statistical properties of the noise through the fluctuation-dissipation theorem, and these are those of a Gaussian white noise [50, 98]. Therefore, the ordinary Langevin equation with a δ-correlated Gaussian noise and constant friction, with or without an external force field, describes only normal diffusion of Brownian particles in a long-time run. A Langevin equation can be used to model anomalous diffusion, however, if additional features are considered. For example, a Gaussian but coloured noise can give rise to anomalous diffusion (both superdiffusion and subdiffusion) in the long-time asymptotics [78] even in the absence of dissipation [75]. Another possibility is to consider diffusion governed by a Gaussian white noise but with a time-dependent friction [77], or generalized Langevin equations with a friction memory kernel [76]. In most of the cases the basic physical ingredient is that the system is not in thermal equilibrium (for instance, we have an external source of noise and the fluctuation-dissipation relation does not hold, or our stochastic process is non-Markovian due to some kind of frictional memory). Apart from this formal long-time asymptotics, it is important to realize that, even if a stationary solution for the probability density of the diffusion process exists, the dynamics of the relaxation to the stationary behaviour

can be very different depending on specific parameters of the system. Our aim now is to study this relaxation dynamics within the classical Langevin equation, to clarify the role of the adiabatic potential and the chaotic dynamics in the relaxation process, as well as the influence of noise and dissipation on the deterministic dynamics.

When introducing dissipation, the stable periodic orbits become sinks or attracting centres [99] and the invariant tori (islands) are destroyed. Both regular and chaotic motions become transient, since eventually all trajectories settle down in one of the sinks (minima at the hollow or the on-top sites). However, the existence of an external force, even if it is random, will eventually provide enough energy for escaping an attractor and give rise to diffusive motion. The addition of weak noise to a non-linear dynamical system can modify considerably its local stability properties, but global stability may be relatively conserved [100]. The noise also influences the transport properties and can induce transitions between different stable steady states [101]. Here we assume the simplest possible model for including friction and temperature, which has also been used in the molecular dynamics simulations of the system, namely a Gaussian white noise with a constant friction, corresponding to a Langevin equation of the type (4.25). In order to avoid strong perturbations of the deterministic dynamics, we keep the noise intensity (temperature) small and the friction constant also small. We have solved the corresponding Langevin equation for different values of friction and temperature, using an accurate fourth-order stochastic Runge–Kutta method [102]. High-order methods are desirable in order to treat properly the part corresponding to the classical dynamics, especially at low values of friction. To give an idea of the changes originated in the chaotic dynamics, we have propagated an ensemble of trajectories with the same initial conditions as were used in figure 2 and calculated again the Poincaré surface of section. This is shown in figure 20(*a*) for $T = 50$ K and friction $\gamma = 10^{-3}$ ps^{-1}. It is seen that the island structure coming from the main parallel diffusing motion around $y = p_y = 0$ (compare to figure 2(*a*)) becomes blurred, but still there are many orbits giving narrow bands around this centre; therefore there is a resemblance to quasiperiodic motion of the free-diffusive type.

As pointed out above, without any additional ingredients in the usual Langevin equation (4.25) the diffusional dynamics is expected to be normal when the time for thermal equilibration is reached, meaning that any effect due to the adiabatic potential is washed out by the frictional coupling. The time needed for that is $\tau_{th} > \gamma^{-1}$. If the friction constant is small enough, it is possible that the thermal equilibration time is much bigger than the equilibration time due to the chaotic dynamics, and under such circumstances one could observe a transient region in the MSD or the power spectrum where the adiabatic or systematic potential plays an important role.

For the values of T and friction used in figure 20(*a*), we have calculated the MSD and power spectrum of a canonical ensemble of trajectories with an initial Maxwell distribution for the velocities, shown in figure 20(*b*). Note that thermal equilibration times are of the order of 10^3 ps, while dynamical equilibrium is reached at about 100 ps. This can be appreciated in the inset, where we can distinguish two different slopes for the MSD, one giving 'transient' anomalous diffusion and the other normal diffusion, and the same can be seen in the behaviour of the power spectrum at small frequencies. Since experimental timescales are finite, this transient anomalous diffusion could be observed in some systems (for this particular one, γ was found to be around 1 ps^{-1} [12] and transient anomalous diffusion cannot be seen). It is worth noting that for diffusion of Xe atoms on a Pt(111) surface the extreme case of ideal-gas behaviour (zero effective friction and no influence of the adiabatic potential, corresponding to ballistic diffusion) has been observed experimentally [103]. Finally, it is also interesting to see that at finite frequencies the power spectrum shows a broad band around $\omega = \omega_0$ (recall that the frequencies in figure 20(*b*) are scaled by ω_0) which is the fingerprint of the frustrated

translational motion. This should be compared to the power spectrum obtained from the deterministic dynamics at $E = 100$ meV, figure 17(a).

6. Conclusions

The classical dynamics can be considered as a starting point, or the simplest level of approximation, for the analysis of vibrational and diffusional transport processes of atoms adsorbed on metal surfaces. Although a quantitative study usually requires the inclusion of some kind of frictional coupling and thermal effects, the detailed investigation of the deterministic dynamics presents some interesting aspects, both for practical and conceptual reasons. First, the role played by the purely adiabatic atom–surface interaction, generally described by a two-dimensional PES, can be better clarified. Since in general the PES can be regarded as non-separable, the dynamics will be complex, showing different degrees of integrability and chaos depending on the energy. Second, the chaotic dynamics by itself can induce different diffusive behaviours. In this respect, it can be seen as a stochastic process and approached within a statistical mechanical framework, developing a theory of transport in phase space. This justifies the use of statistical mechanics for treating transport processes in systems with few degrees of freedom, without the need to introduce a coupling to a thermal bath. Third, the deterministic dynamics can influence considerably the existence of long jumps and explain how they arise in complex potentials. Moreover, it reveals what features of the adiabatic potential can be of relevance for explaining qualitative details of the experiments, such as the existence of long diffusion paths along specific directions. Fourth, it can give rise to diffusion mechanisms different to those usually considered and produce anomalous behaviour (diffusion faster or slower than normal) which could be eventually detectable in different experimental quantities. And fifth, it determines the short-time behaviour including vibrational motions as well as the trends of the system towards equilibrium.

The work presented in this review can be considered as a first step towards a deeper understanding of the role played by the chaotic dynamics in atom–surface diffusion, as well as the possibility of observing anomalous transport in these systems. We envisage several interesting continuations of the work discussed here. From a more theoretical point of view, the relation between the phase-space structure (periodic orbits) and the Pollicott–Ruelle resonances needs to be clarified, using recent mathematical techniques such as trace formulae [9, 104, 105]. Moreover, it is important to see the effect of adding noise to such dynamical resonances. On the other hand, the approaches to atom–surface diffusion discussed here, even the Langevin and FP formalisms, are the simplest ones, since the friction is assumed to be constant and the random force a purely Gaussian white noise. Furthermore, no interaction between adatoms is considered. In a variety of physical situations, one can think of including additional effects. The most obvious one is the effect of coverage—by taking into account adatom interactions. The shape of the quasielastic peak is very sensitive to correlated motions of the adatoms, and a marked increase in the peak width with increasing coverage is observed in the experiments which has not yet been explained theoretically [14]. Another realistic situation that could be considered is non-local effects produced by a time-dependent friction or correlated noise. Retardation effects can be justified if the substrate fluctuations, characterized by the Debye frequency, are of the order of the adatom frequency of vibration, but if adatom–adatom interactions are included, a correlated noise term may also be necessary, which is not considered in the above simulations [14]. We note that in these cases long-time anomalous transport may indeed occur within the Langevin formalism [76–78]. As a last point, when an external (electric or magnetic) field is added, transport properties can change drastically and a non-zero net current (directed transport) may occur, as is the case in surface electromigration [106]. The addition

of an electric field may also serve to enhance and control diffusion [107]. The existence of directed transport in periodic potentials (also called the *ratchet* effect) is being actively studied now; this work is mainly motivated by the basic physical mechanism of operation of biological molecular motors, and the chaotic dynamics may play an important role in such transport [108].

Acknowledgments

RG was supported by a contract *Ramón y Cajal* from the Ministerio de Ciencia y Tecnología, Spain. Financial support from the Ministerio de Ciencia y Tecnología under the project BCM2001-2197 is also acknowledged.

References

[1] Gomer R 1990 *Rep. Prog. Phys.* **53** 917
[2] Lombardo S J and Bell A T 1991 *Surf. Sci. Rep.* **13** 1
[3] Frenken J W M and Hinch B J 1992 *Helium Atom Scattering from Surfaces (Springer Series in Surface Sciences vol 27)* ed E Hulpke (New York: Springer) p 287
[4] Barth J V 2000 *Surf. Sci. Rep.* **40** 75
[5] Kramers H A 1940 *Physica* **7** 284
[6] Hanggi P, Talkner P and Borkovec M 1990 *Rev. Mod. Phys.* **62** 251
[7] Melnikov V I 1991 *Phys. Rep.* **209** 1
[8] Ruelle D 1978 *Thermodynamic Formalism* (Reading, MA: Addison-Wesley)
[9] Gaspard P 1998 *Chaos, Scattering and Statistical Mechanics* (Cambridge: Cambridge University Press)
[10] Dorfman J R 1999 *An Introduction to Chaos in Non-Equilibrium Statistical Mechanics* (Cambridge: Cambridge University Press)
[11] Meiss J D 1992 *Rev. Mod. Phys.* **64** 795
[12] Graham A P, Hofmann F, Toennies J P, Chen L Y and Ying S C 1997 *Phys. Rev. Lett.* **78** 3900
Graham A P, Hofmann F, Toennies J P, Chen L Y and Ying S C 1997 *Phys. Rev.* B **56** 10 567
[13] Ellis J P and Toennies J P 1993 *Phys. Rev. Lett.* **70** 2118
Chen L Y and Ying S C 1993 *Phys. Rev. Lett.* **71** 4361
[14] Cucchetti A and Ying S C 1999 *Phys. Rev.* B **60** 11 110
Ellis J, Graham A P, Hofmann F and Toennies J P 2001 *Phys. Rev.* B **63** 195408
[15] Lindgren S A, Svensson C and Wallden L 1990 *Phys. Rev.* B **42** 1467
[16] Chen L Y and Ying S C 1994 *Phys. Rev.* B **49** 13 838
Chen L Y, Baldan M R and Ying S C 1996 *Phys. Rev.* B **54** 8856
[17] Rejto P and Andersen H C 1993 *J. Chem. Phys.* **98** 7636
[18] Hershkovitz E, Talkner P, Pollak E and Georgievskii Y 1999 *Surf. Sci.* **421** 73
[19] Tabor M 1989 *Chaos and Integrability in Nonlinear Dynamics* (New York: Wiley)
[20] Ott E 1993 *Chaos in Dynamical Systems* (Cambridge: Cambridge University Press)
[21] Wiggins S 1990 *Introduction to Applied Non-Linear Dynamical Systems and Chaos* (New York: Springer)
[22] Weinstein A 1973 *Invent. Math.* **20** 47
[23] See, for instance, Christiansen F 2001 Fixed points, and how to get them *Classical and Quantum Chaos* ed P Cvitanović, R Artuso, R Mainieri, G Tanner and G Vattay (Copenhagen: Niels Bohr Institute) www.nbi.dk/ChaosBook/
Farantos S C 1995 *THEOCHEM* **341** 91
[24] Press W H, Flannery B P, Teukolsky S A and Vetterling W T 1992 *Numerical Recipes* (Cambridge: Cambridge University Press) ch 17
[25] Seydel R 1994 *Practical Bifurcation and Stability Analysis* (New York: Springer)
[26] Meyer K R 1970 *Trans. Am. Math. Soc.* **149** 95
de Aguiar M A M, Malta C P, Baranger M and Davies K T R 1987 *Ann. Phys., NY* **180** 167
[27] Mao J M and Delos J B 1992 *Phys. Rev.* A **45** 1746
[28] Guantes R, Vega J L and Miret-Artés S 2001 *Phys. Rev.* B **64** 245415
[29] Wilson E B Jr, Decius J C and Cross P C 1980 *Molecular Vibrations* (New York: Dover) ch 2
[30] Percival I C 1977 *Adv. Chem. Phys.* **36** 1
[31] Graham A, Hofmann F and Toennies J P 1996 *J. Chem. Phys.* **104** 5311

[32] Percival I C 1979 *Non-Linear Dynamics and the Beam–Beam Interaction* vol 57, ed M Month and J C Herrera (New York: AIP) p 302
[33] Aubry S 1978 *Solitons and Condensed Matter Physics* ed A R Bishop and T Schneider (Berlin: Springer) p 264
[34] Adler D L *et al* P H 1993 *Phys. Rev.* B **48** 17 445
[35] Hansen J-P and McDonald I R 1986 *Theory of Simple Liquids* (London: Academic)
[36] Allen M P and Tildesley D J 1987 *Computer Simulations of Liquids* (Oxford: Clarendon)
[37] Onsager L 1931 *Phys. Rev.* **37** 405
Onsager L 1931 *Phys. Rev.* **38** 2265
[38] Kubo R, Toda T and Hashitsume N 1991 *Statistical Physics* vol 2 (Berlin: Springer)
[39] Chandrasekhar S 1943 *Rev. Mod. Phys.* **15** 1
[40] Kubo R 1962 *J. Math. Phys.* **4** 174
[41] Gardiner C W 1983 *Handbook of Stochastic Methods* (Berlin: Springer)
[42] van Hove L 1954 *Phys. Rev.* **95** 249
[43] Vineyard G H 1958 *Phys. Rev.* **110** 999
[44] Hofmann F, Schölkopf W and Toennies J P 1994 Proc. Welsh Foundation Conf. on Chemical Research (Houston, TX) p 197
Hoffman F and Toennies J P 1996 *Chem. Rev.* **96** 1307
[45] Levi A C, Spadacini R and Tommei G E 1982 *Surf. Sci.* **121** 504
[46] Van Vleck J H 1948 *Phys. Rev.* **72** 1168
[47] Zwanzig R 1960 *J. Chem. Phys.* **33** 1338
[48] Mori H 1965 *Prog. Theor. Phys.* **33** 423
[49] Ala-Nissila T and Ying S C 1992 *Prog. Surf. Sci.* **39** 227
[50] Risken H 1984 *The Fokker–Planck Equation* (Berlin: Springer)
[51] Ferrando R, Spadacini R, Tommei G E and Caratti G 1993 *Physica* A **195** 506
Ferrando R, Spadacini R and Tommei G E 1993 *Phys. Rev.* E **48** 2437
Ferrando R, Spadacini R, Tommei G E and Caratti G 1994 *Surf. Sci.* **301** 411
[52] Pollak E, Bader J, Berne B J and Talkner P 1993 *Phys. Rev. Lett.* **70** 3299
[53] Wanshtröm G 1990 *Interactions of Atoms and Molecules with Solid Surfaces* ed V Bortolani, N H March and N P Tosi (New York: Plenum) p 529
[54] Senft D C and Ehrlich G 1995 *Phys. Rev. Lett.* **74** 294
[55] Sholl D S and Skodje R T 1994 *Physica* D **71** 168
[56] Geisel T, Zacherl A and Radons G 1987 *Phys. Rev. Lett.* **59** 2503
Radons G, Geisel T and Zacherl A 1988 *Z. Phys.* B **71** 117
[57] Richardson L F 1926 *Proc. R. Soc.* **110** 709
[58] Scher H and Montroll E W 1975 *Phys. Rev.* B **12** 2455
[59] Fleischmann R, Geisel T and Ketzmerick R 1992 *Phys. Rev. Lett.* **68** 1367
[60] Doi M and Edwards S F 1986 *The Theory of Polymer Dynamics* (Oxford: Clarendon)
[61] Wu X-L and Libchaber A 2000 *Phys. Rev. Lett.* **84** 3017
[62] Weeks E R and Swinney H L 1998 *Phys. Rev.* E **57** 4915
[63] Bychuk O V and O'Shaughnessy B 1995 *Phys. Rev. Lett.* **74** 1795
[64] Metzler R and Klafter J 2000 *Phys. Rep.* **339** 1
[65] Geisel T, Niertwetberg J and Zacherl A 1985 *Phys. Rev. Lett.* **54** 616
[66] Shlesinger M F and Klafter J 1985 *Phys. Rev. Lett.* **54** 2551
[67] Shlesinger M F, Zaslavsky G M and Frisch U (ed) 1995 *Lévy Flights and Related Topics in Physics* (Berlin: Springer)
[68] Klafter J, Shlesinger M F and Zumofen G 1996 *Phys. Today* **49**(2) 33
[69] Paul W and Baschnagel J 1999 *Stochastic Processes: from Physics to Finance* (Berlin: Springer)
[70] Shlesinger M F, Zaslavsky G M and Klafter J 1993 *Nature* **363** 31
[71] Metzler R and Klafter J 2001 *Adv. Chem. Phys.* **116** 223
[72] Sokolov I M 2000 *Phys. Rev.* E **63** 011104
[73] Feller W 1971 *An Introduction to Probability Theory and its Applications* vol 2 (New York: Wiley)
[74] Fogedby H C 1994 *Phys. Rev.* E **50** 1657
[75] Masoliver J and Wang K G 1995 *Phys. Rev.* E **51** 2987
[76] Wang K G and Tokuyama M 1999 *Physica* A **265** 341
[77] Lillo F and Mantegna R N 2000 *Phys. Rev.* E **61** R4675
[78] Denisov S I and Horsthemke W 2000 *Phys. Rev.* E **62** 7729
[79] Zaslavsky G M and Niyazov B A 1997 *Phys. Rep.* **283** 73

[80] Lutz E 2001 *Phys. Rev. Lett.* **86** 2208
[81] Tsallis C, Levy S V F, Souza A M C and Maynard R 1995 *Phys. Rev. Lett.* **75** 3589
[82] Kaniadakis G and Lapenta G 2000 *Phys. Rev.* E **62** 3246
[83] Lichtenberg A J and Lieberman M A 1992 *Regular and Chaotic Dynamics* (New York: Springer)
[84] Klafter J and Zumofen G 1994 *Phys. Rev.* E **49** 4873
[85] Shlesinger M F, West B J and Klafter J 1987 *Phys. Rev. Lett.* **58** 1100
[86] Klafter J, Blumen A and Shlesinger M F 1987 *Phys. Rev.* A **35** 3081
[87] Geisel T, Wagenhuber J, Niebauer P and Obermair G 1990 *Phys. Rev. Lett.* **64** 1581
Geisel T, Wagenhuber J, Niebauer P and Obermair G 1992 *Phys. Rev.* B **45** 4372
[88] Van Kampen N G 1996 *Stochastic Processes in Physics and Chemistry* (Amsterdam: North-Holland)
[89] Ruelle D 1986 *Phys. Rev. Lett.* **56** 405
[90] Isola S 1988 *Commun. Math. Phys.* **116** 343
[91] Bouchaud J P and Georges A 1990 *Phys. Rep.* **195** 127
[92] Kutner R 1999 *Physica* A **264** 84
[93] Chudley C T and Elliott R J 1961 *Proc. Phys. Soc.* **77** 353
[94] Gradstein I S and Ryzhik I M 1994 *Tables of Integrals, Series and Products* (Boston, MA: Academic)
[95] Compte A 1996 *Phys. Rev.* E **53** 4191
[96] Samko S G, Kilbas A A and Marichev O I 1993 *Fractional Integrals and Derivatives. Theory and Applications* (New York: Gordon and Breach)
[97] Sokolov I M, Klafter J and Blumen A 2001 *Phys. Rev.* E **64** 021107
[98] Reimann P 2001 *Chem. Phys.* **268** 337
[99] Lieberman M A and Tsang K Y 1985 *Phys. Rev. Lett.* **55** 908
[100] Crutchfield J P, Farmer J D and Huberman B A 1982 *Phys. Rep.* **92** 45
[101] Landa P S and McClintock P V E 2000 *Phys. Rep.* **323** 1
[102] Hershkovitz E 1998 *J. Chem. Phys.* **108** 9253
Honeycutt R L 1992 *Phys. Rev.* A **45** 600
[103] Ellis J, Graham A P and Toennies J P 1999 *Phys. Rev. Lett.* **82** 5072
[104] Cvitanović P, Artuso R, Mainieri R, Tanner G and Vattay G *Classical and Quantum Chaos* (Copenhagen: Niels Bohr Institute) www.nbi.dk/ChaosBook/
[105] Khodas M and Fishman S 2000 *Phys. Rev. Lett.* **84** 2837
Weber J, Haake F and Seba P 2000 *Phys. Rev. Lett.* **85** 3620
[106] Derényi I, Lee C and Barabási A L 1998 *Phys. Rev. Lett.* **80** 1473
de Pablo P J, Colchero J, Gómez-Herrero J, Asenjo A, Luna M, Serena P A and Baró A M 2000 *Surf. Sci.* **464** 123
[107] Talkner P, Hershkovitz E, Pollak E and Hänggi P 1999 *Surf. Sci.* **437** 198
Reimann P, Van den Broeck C, Linke H, Hänggi P, Rubi J M and Pérez-Madrid A 2001 *Phys. Rev. Lett.* **87** 010602
[108] For a recent account, see Reimann P 2002 *Phys. Rep.* **361** 57